Probing the force-from-lipid mechanism with synthetic polymers

Miranda L. Jacobs[1,2], Jan Steinkühler[1], Audra Lemley[3], Megan J. Larmore[4], Leo C. T. Ng[4], Stephanie M. Cologna[3], Paul G. DeCaen[4]*, Neha P. Kamat[1,2]*

1. Department of Biomedical Engineering, Northwestern University, Evanston, Illinois, USA.
2. Center for Synthetic Biology, Northwestern University, Evanston, IL 60657, USA
3. Department of Chemistry, University of Illinois Chicago, Chicago, IL, USA.
4. Department of Pharmacology, Feinberg School of Medicine, Northwestern University, Chicago, Illinois, USA.

Abstract

A central feature of mechanotransduction is the ability of mechanosensitive channels to respond to mechanical deformation of the surrounding lipid bilayer. Accordingly, the mechanical properties of membranes should play an important role in modulating force transmission to embedded channels, yet this relationship remains unknown for a wide class of mechanosensitive channels across prokaryotic and eukaryotic systems. Here, we use a synthetic amphiphile to modulate the membrane mechanical properties of cell-derived vesicles. Using precise membrane mechanical characterization techniques that have rarely been used in conjunction with electrophysiology techniques, we uncover two key membrane properties that affect the activation of *E. coli* mechanosensitive channel of large conductance (MscL). Our study reveals that decreases in the membrane area expansion modulus, K_A, and bending rigidity, k_c, lead to increases in the pressure required to activate MscL and that this effect is reproducible with the mammalian channel, TREK-1. Together, our results bolster the *force-from-lipids* mechanism by demonstrating that changes in membrane mechanical properties, induced through distinct membrane amphiphiles, similarly impact the gating force of MscL and TREK-1. In addition, our results reveal the capacity of membrane amphiphiles to alter the activity and sensitivity of mechanosensitive channels through changes in long-range force transmission.

Introduction

Mechanosensitive channels are a class of membrane proteins which are found in all domains of life and play important roles ranging from cellular volume regulation to touch and hearing sensation (Brohawn et al., 2019; Cahalan et al., 2015; Cox et al., 2019; Dave et al., 2021; del Mármol et al., 2018; Procko et al., 2021; Sun et al., 2019; Vásquez et al., 2014; Wang et al., 2021). Many mechanosensitive channels are thought to transduce mechanical forces into biochemical signals by responding to tension in the lipid bilayer, referred to as the *force-from-lipids* mechanism (Guo and MacKinnon, 2017; Martinac et al., 2020; Reddy et al., 2019; Ridone et al., 2018; Teng et al., 2015). Through this mechanism, mechanosensitive channels are proposed to be affected by long-range mechanical forces in the membrane that affect the bilayer lateral pressure profile (Anishkin et al., 2014; Bruno et al., 2007; Cordero-Morales and Vásquez, 2018). As membrane tension can propagate distances of tens of microns within seconds in motile cells and axons (Houk et al., 2012; Shi et al., 2022), and the diffusion of tension relies directly on membrane properties (Cohen and Shi, 2020), lipid components that alter membrane mechanical properties should alter force transmission and impact the activation of embedded mechanosensitive channels (Johnson, 2015). Towards this idea, various studies have begun to demonstrate the relationship between membrane composition and mechanosensitive channel function and have shown that changes in membrane composition may modulate force propagation to embedded channels (Brohawn et al., 2014; Caires et al., 2017; Nakayama et al., 2018; Nomura et al., 2012; Ridone et al., 2018). Yet, the mechanism of how many membrane

amphiphiles impact mechanosensitive channels remains unknown. This is in large part because we have been unable to directly measure and determine the relative contributions of different membrane mechanical properties to mechanosensitive channel activation.

One reason it has been difficult to directly resolve the role of membrane mechanical properties in mechanosensitive channel activation is that certain membrane mechanical properties are difficult to measure. Another reason is that it can be difficult to significantly change membrane properties using lipids alone in a way to isolate or probe their impact on channel activation. Towards the former, a variety of studies have proposed that the alteration of membrane properties, through changes in membrane composition, affects mechanosensitive function (Anishkin et al., 2014; Balleza, 2012; Bruno et al., 2007; Caires et al., 2017; Lundbæk et al., 2010, 2004; Ridone et al., 2020, 2018; Romero et al., 2019; Xue et al., 2020). Through these studies, the impact of various membrane properties such as area expansion modulus (K_A), the extent to which the membrane stretches in response to tension, bending stiffness (k_c), the energy required to bend and smooth thermal fluctuations in a membrane, fluidity, a measure of viscosity or the lateral diffusion of lipids in a membrane, and hydrophobic thickness, the length of the hydrophobic core of the membrane, have been proposed to play a role in mechanosensitive channel behavior (Caires et al., 2017; Nakayama et al., 2018; Ridone et al., 2018; Romero et al., 2019). Yet, most of these studies have relied on published estimates or used methods which measure the bulk property of a cell that include cytoskeletal mechanics. Towards the latter reason, the direct role of certain membrane mechanical properties on mechanosensitive channel behavior has been difficult to discern in the presence of natural lipids. Phospholipids, which are the most abundant class of lipids in living systems, impart small changes to the area expansion modulus, which is expected to play a significant role in the activation of channels regulated by a force-from-lipid mechanism. The effect of these small changes on mechanosensitive channel behavior is often difficult to distinguish from changes in other membrane properties. However, non-natural amphiphiles, like poloxamers have the ability to alter membrane properties to a greater extent than natural lipids. By using membrane amphiphiles that change the membrane properties in unique and amplified ways, we can better distinguish the impact of a specific property on protein function.

Here, we reveal a relationship between membrane elasticity and bending rigidity and the pressure required to activate *E. coli* MscL. Using giant plasma membrane vesicles (GPMVs), poloxamer analogues, voltage-clamp electrophysiology studies, and a series of mechanical characterization techniques, we demonstrate a general role of certain membrane properties in modulating mechanosensitive channel activation. Our results highlight a critical role of membrane amphiphiles in indirectly regulating channel activity via changes in the bulk biophysical properties of membranes, with important implications in defining a mechanism of force-sensing in various living systems from bacterial to neuronal mechanotransduction. As poloxamers are also a kind of nanoplastic, we also comment on the potential impact of nanoplastics on cellular health through interaction with cellular membranes.

Results

We prepared GPMVs, which allow for both assessment of mechanosensitive ion channel activity and membrane mechanical properties (Steinkühler et al., 2021, 2019). GPMVs not only incorporate membrane proteins of interest, but also maintain biological membrane composition and have an overall larger size (>5 µm) required for mechanical characterization via micropipette aspiration, while excluding organelles and cytoskeletal structures that might interfere with measurements of membrane mechanical properties (Figure 1A) (Keller et al., 2009; Levental et al., 2016; Steinkühler et al., 2019). We chose to first focus on the Mechanosensitive Channel of Large Conductance (MscL), which serves as a model mechanosensitive channel (Chang et al.,

1998; Wang et al., 2014). Specifically, we used a gain of function MscL missense mutation, G22S, as opposed to MscL wild-type (WT), due to the lower activation threshold of the former which increased the number of GPMVs with pressure-gated MscL currents (Figure 1-figure supplement 1A) (Heureaux et al., 2014). We created U2OS cell lines stably expressing an MscL-green fluorescent protein (GFP) fusion protein (Figure 1-figure supplement 2), and induced GPMV formation by adding a vesiculation agent (Figure 1-figure supplement 3). We elected to use N-ethylmaleimide (NEM) rather than the more commonly used paraformaldehyde/ dithiothreitol (PFA/DTT) formulation as the latter results in crosslinking of membrane components (Sezgin et al., 2012) and may prevent mechanosensitive channel activation (Figure 1-figure supplement 4).This method also enables the incorporation of membrane additives to modulate membrane mechanical properties (Figure 1-figure supplement 5).The addition of this agent resulted in GPMVs containing MscL visualized by GFP fluorescence and that were an appropriate size for micropipette aspiration measurements (Figure 1A).

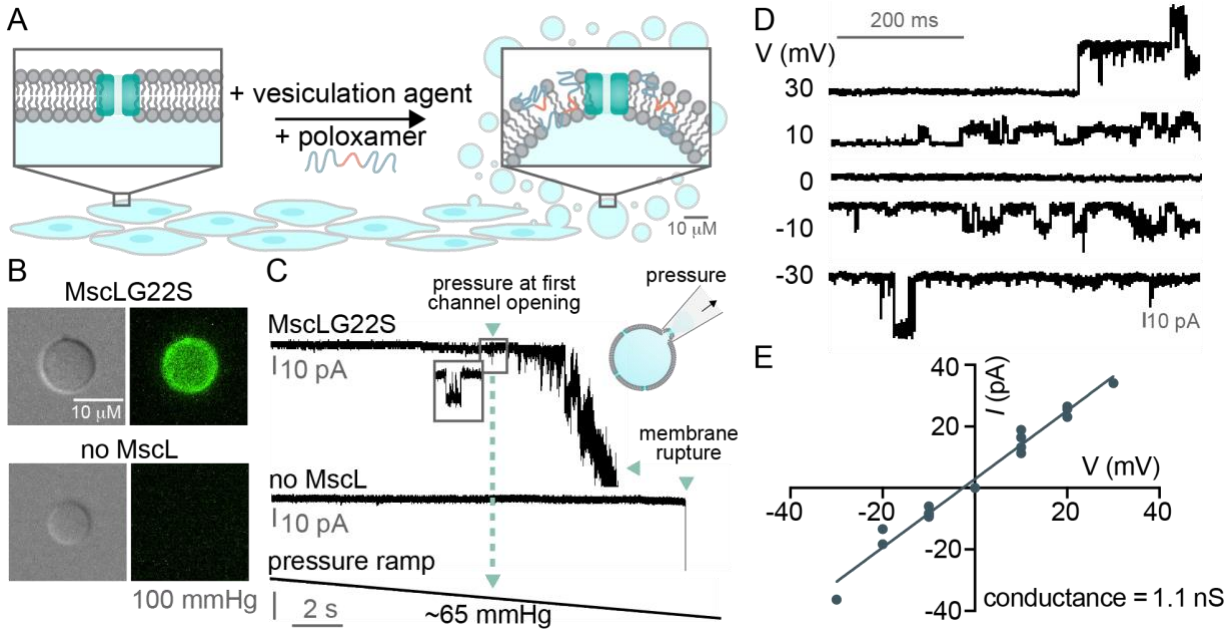

Figure 1. Patch-clamp electrophysiology of giant plasma membrane vesicles (GPMVs) measures MscL pressure sensitivity. A) Schematic representation of GPMV formation. Human bone osteosarcoma epithelial cells (U2OS) containing MscL treated with N-ethylmaleimide vesiculation agent and poloxamer to form GPMVs that contain MscL GFP and the poloxamer into GPMVs containing the channel. B) Microscopy images of GPMVs that are untransfected (bottom) or contain MscLG22S tagged with GFP (top). DIC images (left) and GFP epifluorescence (right) are shown. 10 μM scale bar. C) Representative electrophysiology traces of MscL pressure sensitivity. MscLG22S (top) recordings show MscL activation in response to pressure ramp (bottom). MscL activation sensitivity is defined as the pressure at which the first MscL channel activates. Untransfected GPMVs (no MscL) exhibit no change in current in response to pressure. MscLG22S pressure response is determined by the pressure at first channel opening (ex.~65 mmHg for the shown GPMV). Recordings are performed at -10 mV in 10 mM HEPES pH 7.3, 150 mM NaCl, 2 mM $CaCl_2$. Pipette internal solution consists of 10 mM HEPES pH 7.3, 100 mM NaMES, 10 mM Na_4BAPTA, 10 mM NaCl, 10 mM EGTA. D) Example MssLG22S single channel events recorded from GPMVs derived from U2OS cells. E) Resulting single channel current-voltage relationship used in determination of the MscLG22S conductance. The current amplitude at each voltage (shown in D) is plotted and the slope of the linear fit was used to determine channel conductance. MscLG22S conductance is 1.113 nS (95% confidence 1.020 to 1.207 nS), n = 17 individual recordings at various holding potentials.

We validated the presence and activity of MscLG22S in GPMVs via florescence microscopy using a C-terminal GFP tag, which was observable in our GPMV membranes (Figure 1B). Following this confirmation, we assessed MscLG22S activation sensitivity using patch-clamp electrophysiology techniques with an integrated pressure controller and quantified MscLG22S sensitivity using the pressure at first channel opening (Figure 1-figure supplement 6) (Nomura et al., 2012). We applied a pressure ramp that reached suction pressures above 160 mmHg and observed pressure-induced channel activation in our GPMVs that contained MscLG22S, while no currents were observed in our control GPMVs which lacked MscLG22S (Figure 1C, Figure 1-figure supplement 7). We measured channel conductance by quantifying the current through individual MscLG22S channels under different voltages (Figure 1D). We found the conductance of *E. coli* MscLG22S and MscLWT to be ~1 nS in GPMVs (Figure 1E, Figure 1-figure supplement 1B), which is similar to published values of MscL conductance in mammalian cells (Doerner et al., 2012) and bacterial membranes (Sukharev et al., 1999, 1994). In addition, we confirmed that MscLG22S was sensitive to membrane composition in our GPMV platform through the addition of a curvature-inducing amphiphile, lysophosphtidylcholine (LPC) as described previously (Figure 1-figure supplement 8) (Nomura et al., 2012). These observations confirmed that the stochastic channel currents we observed were due to pressure-induced MscLG22S activation and MscLG22S is sensitive to membrane composition in GPMVs, similar to other membrane platforms.

Poloxamer P124 reduces the pressure-sensitivity of MscL

After characterizing the behavior of MscLG22S in GPMVs, we next set out to determine the effect of various membrane mechanical properties on MscLG22S activation sensitivity. To modulate membrane properties, we used a poloxamer, which is an amphiphilic triblock copolymer that can integrate into bilayer membranes (Figure 2A) (Großkopf et al., 2021). We included increasing amounts of poloxamer 124 (P124) in the buffer during GPMV formation (Figure 1A) and measured MscLG22S activation pressure of the vesicles using patch-clamp electrophysiology. To confirm that poloxamer integrates into the membrane, we used MALDI-MS and observed that two types of selected poloxamers, P124 and P188, integrate into membranes (Figure 2-figure supplement 1). Using microscopy, we found that poloxamer addition increases GPMV surface area (Figure 2-figure supplement 2). In addition, we found that P124 increases GPMV stability consistent with previous studies (Figure 2-figure supplement 3) (Calori et al., 2022). Together, these results suggest that poloxamer readily integrates into GPMV membranes.

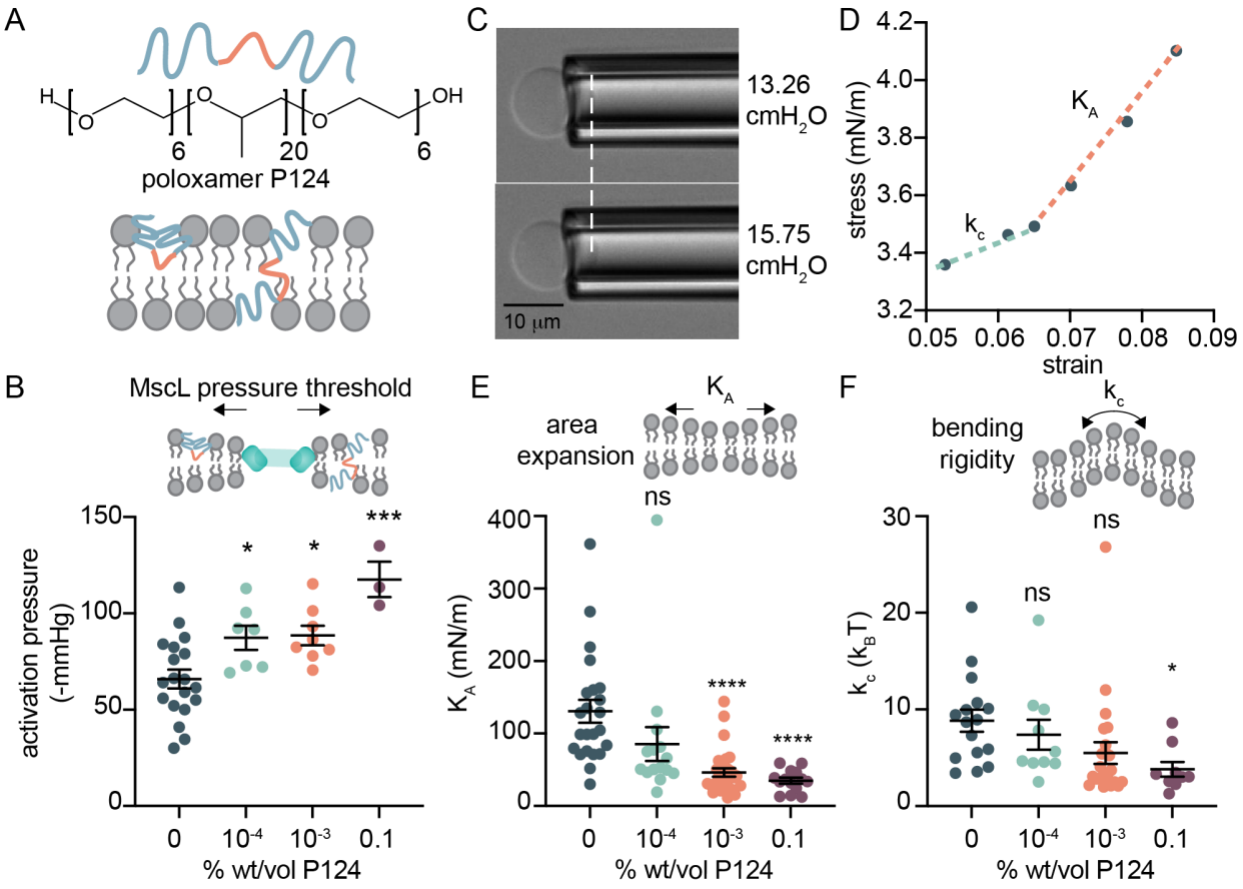

Figure 2. Poloxamer P124 decreases MscL sensitivity and modulates K_A and k_c. A) Schematic and chemical structure of poloxamer P124. Poloxamer may be found in a hairpin or transverse conformation within the membrane. B) MscLG22S activation is desensitized in the presence of P124. MscLG22S activation is defined here as the pressure where the first MscLG22S channel is activated. The pressure at first channel opening was measured for GPMVs prepared in solutions containing 0 – 0.1% wt/vol P124, n ≥ 13 independent GPMVs were recorded. C) Images of micropipette aspiration of GPMVs measuring membrane mechanical properties. Micropipette aspiration is used to measure membrane areal changes in response to applied tension. The area expansion modulus (K_A) and bending rigidity (k_c) of GPMV membranes treated with poloxamer were measured. D) Sample aspiration curve from a micropipette aspiration experiment. A stress-strain curve was plotted to calculate K_A and k_c of GPMV membranes using micropipette aspiration techniques at high and low tension, respectively. E, F) K_A and k_c decrease in the presence of P124. GPMV K_A and k_c were measured using micropipette aspiration techniques after treatment of P124 in the GPMV formation buffer. k_c and K_A were calculated at low- and high-pressure regimes, respectively where K_A is corrected for relaxation of thermal undulations using mean k_c. P124 % wt/vol is as listed, pH 7.3. Bath and pipette solution consist of 10 mM HEPES pH 7.3, 150 mM NaCl, 2 mM $CaCl_2$ in micropipette aspiration studies. Mean activation pressure, K_A, k_c are plotted with error bars that represent standard error of the mean. p-values in B, E, and F were generated by ANOVA using Dunnett's multiple comparisons test compared to no poloxamer. **** $p \leq 0.0001$, *** $p \leq 0.001$, * $p \leq 0.05$, non-significant (ns) $p > 0.05$, $n > 10$.

We found that MscLG22S required higher pressures to activate when GPMVs contained P124 and this response was monotonic with increasing poloxamer concentration, indicating that P124 decreased the sensitivity of MscLG22S (Figure 2B). To further determine MscLG22S sensitivity in the presence of P124, we quantified the percent of GPMVs that contained MscLG22S currents out of all recorded GPMVs which exhibited GFP fluorescence. In this quantification, we only

monitored currents up to a maximum pressure above -80 mmHg, under which we would normally expect MscLG22S activation in a poloxamer-free membrane. We found in GPMVs with the highest buffer concentration of P124 (0.1% wt/vol), only ~20% of GPMV recordings contained active MscLG22S currents, indicating that MscLG22S was not activating in ~80% of GPMVs prepared in high concentrations of P124 (Figure 2-figure supplement 4). Together, these results suggest that the pressure sensitivity of MscLG22S is reduced in the presence of P124 and increases in P124 content eventually leads to the absence of activation of a large fraction of channels.

We then investigated how P124 altered GPMV mechanical properties. Using micropipette aspiration techniques, we measured the area expansion modulus (K_A) (Jacobs et al., 2021) and bending rigidity (k_c) (Rawicz et al., 2000) of GPMVs treated with P124 for greater than 4 hours (Figure 2C, D; Figure 2-figure supplement 5). We found that membrane K_A and k_c decreased with increasing P124 concentration in the buffer (Figure 2E, F). We then measured P124 fluidity using fluorescence anisotropy techniques and did not observe a significant change in membrane fluidity in the presence of P124 (Figure 2-figure supplement 6).

We wondered how these changes in mechanical properties induced by P124 may affect mechanosensitive channel behavior. To assess this relationship, we plotted MscLG22S activation pressure as a function of each of these membrane mechanical property measurements and found that decreases in membrane K_A and k_c correlate with commensurate increases in MscLG22S activation pressure, r = -0.89 and -0.99, respectively (Figure 2-figure supplement 7A, B). However, we found little correlation between membrane fluidity and MscLG22S activation sensitivity, r = 0.37 (Figure 2-figure supplement 7C). These results suggest that MscLG22S reduced sensitivity to pressure in the presence of P124 may be related to the alteration of specific membrane mechanical properties.

Various poloxamers and a detergent reveal a relationship between K_a, k_c and MscL activation sensitivity

To further explore the generality of the relationship between membrane mechanical properties and MscLG22S activation sensitivity, we used a chemically distinct detergent and an expanded set of poloxamers. We selected the detergent $C_{12}E_8$, which is known to decrease membrane K_A (Jacobs et al., 2019; Otten et al., 2000), and measured the effect of this molecule on MscLG22S activation sensitivity. Similar to our results in the presence of P124, $C_{12}E_8$ increased the pressure required to activate MscLG22S (Figure 3-figure supplement 1A). We then measured the mechanical properties of GPMVs treated with $C_{12}E_8$ and confirmed that this molecule has a softening effect on membranes, reducing the K_A and k_c and fluidity (Figure 3-figure supplement 1B, C, D). We then measured the effect of other poloxamers with similar chemical structures but differing molecular weights on MscLG22S pressure sensitivity and membrane mechanical properties (Figure 1-figure supplement 5, Figure 3-figure supplement 2, 3). We plotted the activation pressure of MscLG22S as a function of K_A, k_c, and fluidity for each of the amphiphiles in which we measured both MscLG22S activation and membrane properties and found similar trends as when we evaluated these relationships for each amphiphile individually (Figure 3, Figure 3-figure supplement 4, Figure 2-figure supplement 7). We found that membrane K_A (r = -0.71) (Figure 3A) and k_c (r = -0.81) (Figure 3B) correlated with MscLG22S activation pressure, however, as we observed in the GPMVs containing P124, fluidity did not correlate as well with MscLG22S activation pressure (r = 0.15) (Figure 3C). Taken together, these results confirm that MscLG22S behavior is sensitive to changes in membrane properties where membranes with reduced K_A and k_c generally decrease the pressure sensitivity of MscLG22S (Figure 3D).

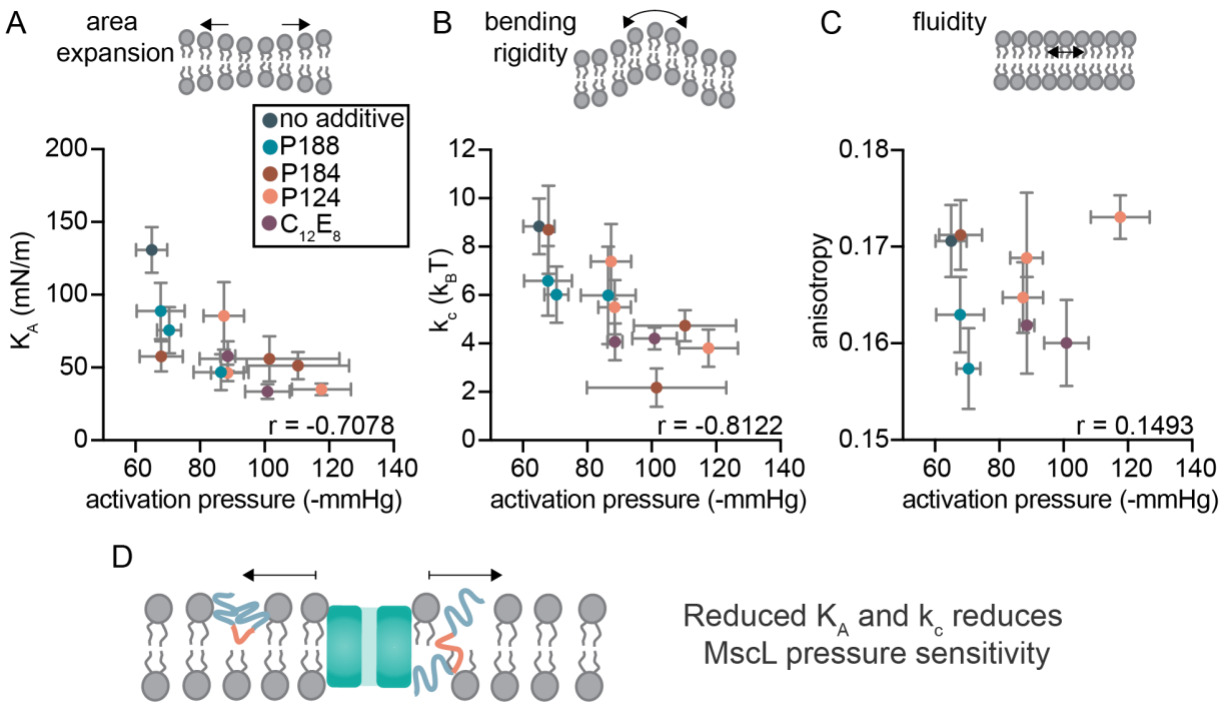

Figure 3. Membrane area expansion modulus and bending rigidity are good predictors for MscL pressure sensitivity. A, B, C) Membrane K_A and k_c, but not fluidity, predict MscLG22S activation pressure. GPMVs were treated with various poloxamers and a detergent ($C_{12}E_8$) during formation and membrane properties (K_A, k_c, and fluidity) and MscLG22S pressure sensitivity were measured. Mean K_A (A), k_c (B), and fluidity (C) are reported as a function of MscLG22S activation pressure when treated with the same amphiphile at a given concentration. For all plots, Pearson's r was used to determine correlation strength, n > 10. D) Potential Mechanism for MscLG22S sensitivity reduction in the presence of membrane-elastizing molecules. MscLG22S activation is modulated by membrane mechanical properties where changes in K_a and k_c alter membrane force propagation and more elastic membranes desensitize MscLG22S.

P124 does not alter MscL activity through pore occlusion or changes in membrane thickness

Next, we sought to rule out the possibility that P124 modulates MscLG22S through a mechanism other than altering membrane mechanical properties. We first hypothesized that P124 could modulate MscLG22S through pore occlusion (Figure 4A). As MscLG22S conductance depends directly on pore size when measured in identical buffer conditions, a decrease in conductance would be expected if P124 resides within the MscLG22S pore (Banerjee et al., 2013; Rokitskaya et al., 2017). We measured the conductance of MscLG22S in the presence of increasing amounts of P124 and found that MscLG22S conductance was not affected by P124 (Figure 4B, C). We included $C_{12}E_8$ as a control which is chemically distinct from poloxamer and would therefore not be expected to interact with MscLG22S in the same way and found that $C_{12}E_8$ also did not affect MscLG22S conductance. Together, these observations demonstrate that P124 and $C_{12}E_8$ do not reside within the MscLG22S pore while in the active conformation.

To further address the possibility that P124 alters MscL activation through pore occlusion, we measured the propensity of P124 to alter activation of a chemically-inducible mutant of MscL that is insensitive to pressure. A mutation within the pore of MscL serves as a hydrophobic gate (G22C) which can be activated by the addition of [2-(trimethylammonium)ethyl] methanethiosulfonate bromide (MTSET), a chemical which forcibly hydrates the pore by introducing charge, (Yoshimura et al., 2001). We hypothesized that if P124 occluded the MscL

pore, MTSET would be unable to open the MscLG22C channel. To assess MscLG22C opening in GPMVs upon MTSET binding, we monitored Ca^{2+} influx via a fluorescent Ca^{2+} indicator, Fluo4. We first validated this assay by ensuring that internal vesicle fluorescence, indicating Ca^{2+} influx, increased only in the presence of the chemically activatable mutant of MscL G22C, and not the pressure sensitive mutant G22S, when MTSET was present (Figure 4D, Figure 4-figure supplement 1). We then determined if MscLG22C chemical activation was altered by P124 addition by quantifying the internal fluorescence of GPMVs containing P124 in the presence of MTSET. This assay showed that P124 did not inhibit MscLG22C activation relative to the no P124 control (Figure 4E) and all conditions resulted in increases in Ca^{2+}-induced fluorescence relative to the MTSET-insensitive control. Taken together, these results suggest that P124 does not occlude the MscL pore

Another potential mechanism by which MscLG22S activation could be altered in the presence of P124 is through increased membrane thickness (Figure 4F). MscL is known to be sensitive to membrane thickness where thinner membranes reduce the gating threshold of MscL (Ridone et al., 2018) and thicker membranes desensitize MscL (Nomura et al., 2012; Ridone et al., 2018). We do not expect membrane thickness to be increased in the presence of poloxamer based on our bending rigidity measurements, because the reduced k_c values suggests a decreased membrane thickness (Figure 3B. However, to further investigate this hypothesis, we performed molecular dynamics simulations to measure changes in membrane thickness, surface area, and K_A after P124 incubation (Figure 4G). Our simulations demonstrated that P124 inserts into the bilayer and this integration increases surface area (Figure 4H) and reduces membrane K_A (Figure 4-figure supplement 3) but does not alter membrane thickness (Figure 4I).

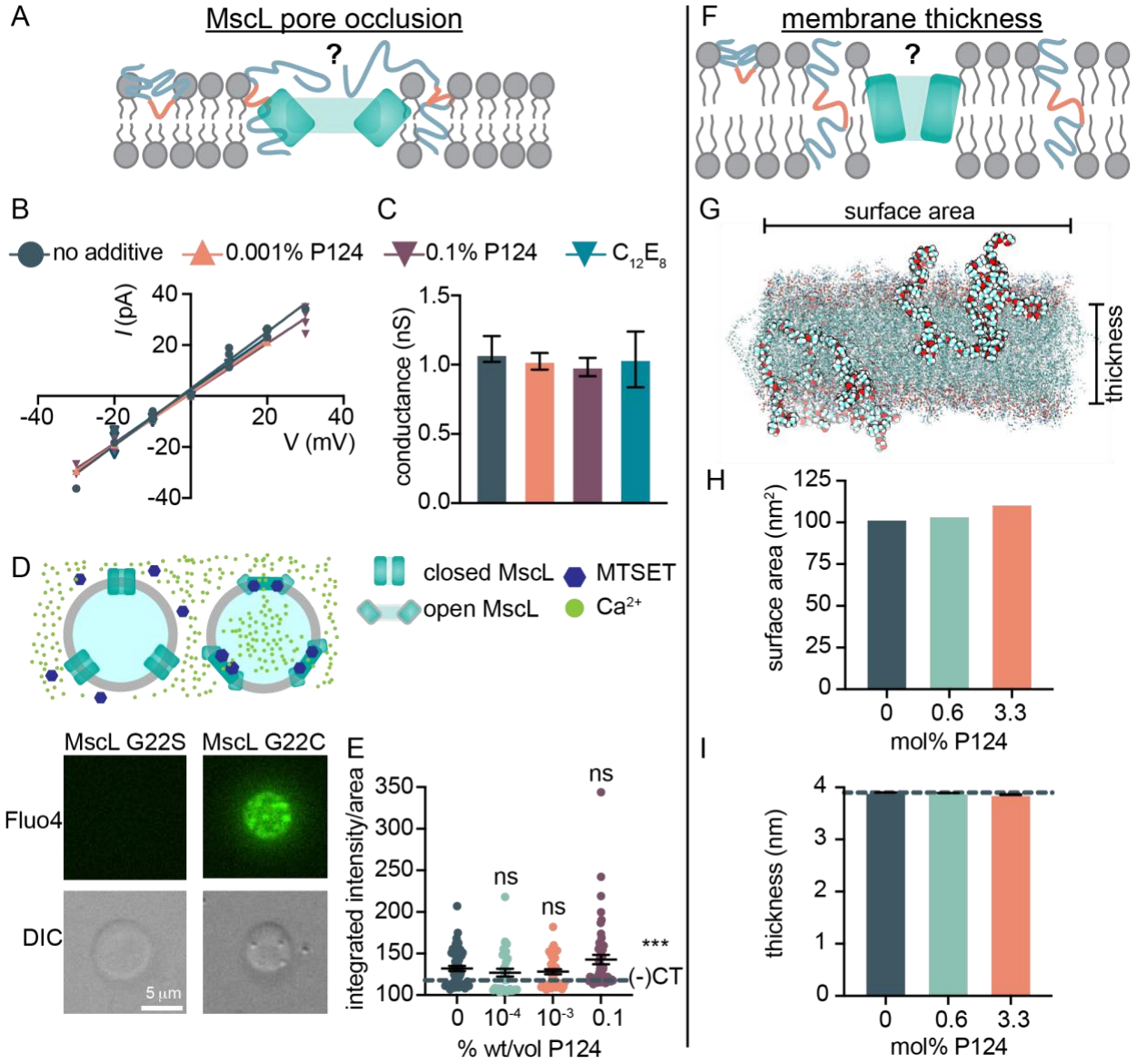

Figure 4. Poloxamer does not impact MscL through pore occlusion or membrane thickness changes. A) Poloxamers may prevent MscLG22S activation through occlusion. B) MscLG22S pore size does not change in the presence of P124. MscLG22S conductance in the presence of P124 is plotted. $C_{12}E_8$ serves as a non-polymeric control. C) MscLG22S conductance quantification in the presence of P124 and $C_{12}E_8$. Mean conductance and 95% confidence interval are plotted from the linear fit shown in panel B. D) Chemical activation of MscLG22C. Fluo4 Ca^{2+} imaging of the internal space of the vesicle reveals that Ca^{2+} influx can be detected when MscLG22C is activated with MTSET but not in the presence of MscLG22S ((-)CT). DIC images show GPMV outline. E) P124 does not prevent MscL activation. GPMVs containing MscLG22C were formed in the presence of various P124 concentrations as indicated. Fluo4 fluorescence was quantified after GPMV incubation with MTSET and 5 mM Ca^{2+} and is plotted as integrated intensity/ vesicle area. Mean is plotted with standard error off the mean. *** $p \leq 0.001$, non-significant (ns) $p > 0.5$, $n > 30$ vesicles per condition. p-values were generated by ANOVA using Dunnett's multiple comparisons test compared to no poloxamer. F) Poloxamers may prevent MscLG22S activation by increasing membrane thickness. G) Schematic of coarse-grain molecular dynamics simulations of DOPC bilayers (translucent) containing P124 (opaque). H) Membrane surface area increases with increasing poloxamer concentration. I) P124 does not increase membrane thickness in molecular simulations. Error bars represent standard error of the mean, n = 3.

TREK-1 confirms the relationship between K_A, k_c and *force-from-lipids* gating of mechanosensitive channels

Finally, we sought to explore the generality of our findings with another mechanosensitive channel. We chose to measure the effect of P124 on the mouse potassium channel, TWIK-related K+ channel 1 (TREK-1), a mechanosensitive channel found in neurons which has been demonstrated to be activated by force-from-lipids and is sensitive to changes in membrane composition (Brohawn et al., 2014). Using a similar expression scheme as MscL, we created stable cell lines of TREK-1 tagged with mEGFP (Figure 5-figure supplement 1), which was retained in the membrane after GPMV formation (Figure 5-figure supplement 2). We observed TREK-1 single-channel currents in response to a pressure gradient using an integrated pressure controller. Similar currents were not observed in untransfected cells, lacking the channel, and exposed to the same experimental conditions (Figure 5A, Figure 5-figure supplement 3). We measured TREK-1 conductance using voltage-clamp electrophysiology measuring the respective current through a single channel and observed an outward conductance of 140 pS, similar to the conductance of TREK-1 in cellular systems (Figure 5B) (Heurteaux et al., 2004; Xian Tao Li et al., 2006). The inward conductance was undetectable below +50 mV, suggesting a primarily outward rectifying channel, consistent with previous observations (Xian Tao Li et al., 2006). We next determined if TREK-1 activation pressure was altered by P124. We treated TREK-1-containing GPMVs with P124 and observed an increase in the pressure required to activate the first TREK-1 channel (Figure 5C). Again, the chemically distinct $C_{12}E_8$ amphiphile also increased the channel activation pressure (Figure 5C), similar to our results with MscL (Figure 2B, Figure 3-figure supplement 1A). Finally, we wondered if TREK-1 activation could be predicted by membrane properties. We plotted K_a, k_c, and fluidity as a function of TREK-1 activation pressure. Similar to MscL, we observed a strong correlation between TREK-1 activation pressure and K_A ($r = -0.99$) and k_c ($r = -0.97$) (Figure 5D, E). As we observed in the presence of MscL, there was not a correlation between membrane fluidity and TREK-1 activation pressure ($r = -0.50$) (Figure 5F). These results suggest a relationship between membrane elastic properties, K_A, and k_c, and TREK-1 activation sensitivity. Taken together, our observations suggest that alteration of these mechanical properties are sufficient to alter mechanosensitive channel activation as exhibited by the capacity of various poloxamer analogs and a chemically distinct detergent to alter mechanosensitive channel activation pressure.

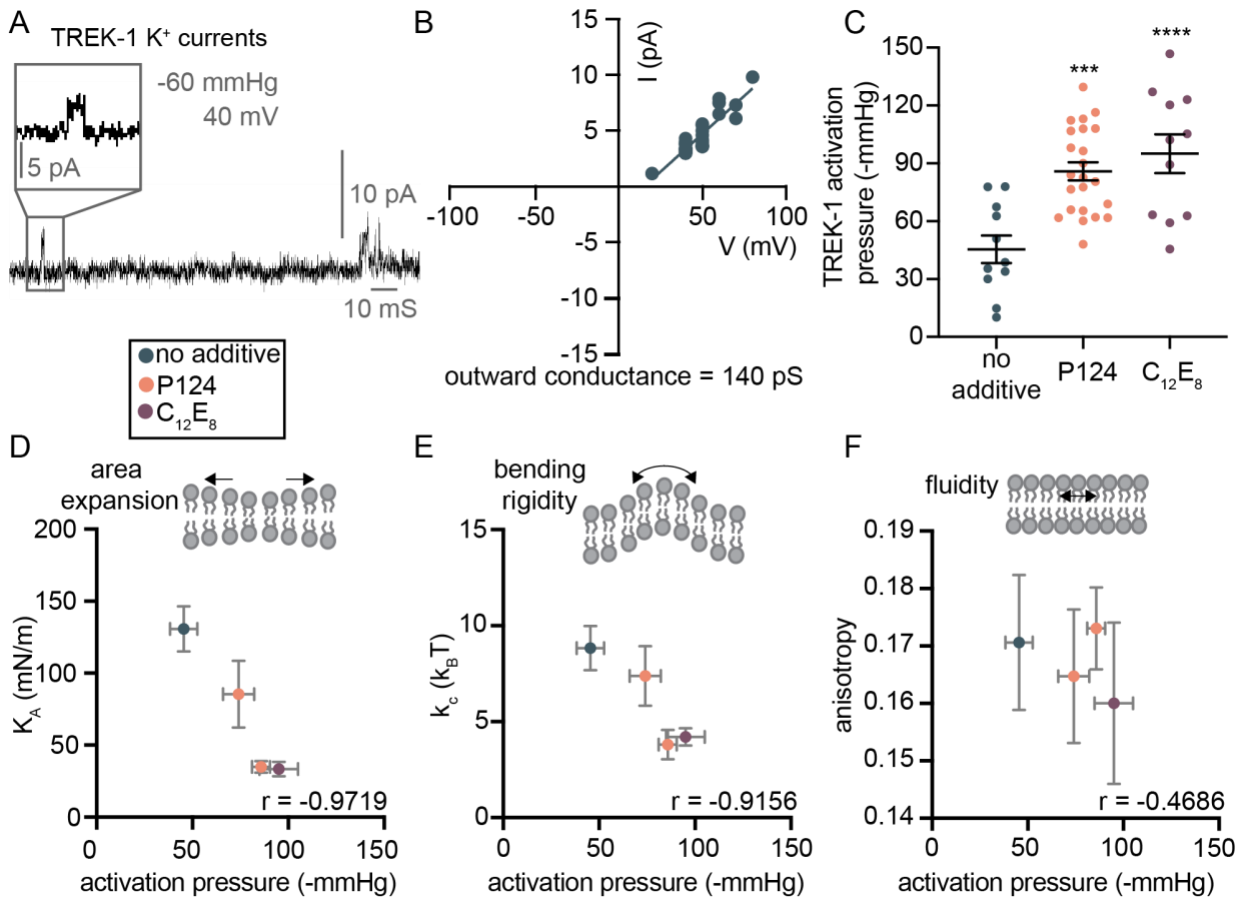

Figure 5. TREK-1 activation is also predicted by membrane properties. A) Mouse TREK-1 single-channel potassium currents are observed GPMVs in response to pressure. TREK-1 currents were measured using patch-clamp electrophysiology with an integrated pressure controller in asymmetric potassium conditions, pH 7.3. B) TREK-1 is outward rectifying with a conductance of 140 pS. TREK-1 current was quantified under various holding potentials. TREK-1 currents were larger under negative voltages and the slope of the I/V relationship under negative voltages was used to measure outward rectifying conductance. Individual electrophysiology measurements are plotted, n > 15. C) TREK-1 activation pressure is increased in the presence of a poloxamer (0.1% P124) and a detergent (1 μm $C_{12}E_8$). Mean activation pressure is plotted and dots represent individual measurements, error bars represent standard error of the mean. p-values were generated by ANOVA using Dunnett's multiple comparisons test compared to no poloxamer. **** $p \leq 0.0001$, *** $p \leq 0.001$, n>10. D, E) Membrane K_A and k_c predict TREK-1 activation pressure. GPMVs were treated with P124 or $C_{12}E_8$ at the highest concentration and TREK-1 activation or membrane mechanical properties were measured. Mean K_a or k_c and TREK-1 activation pressure were plotted. F) Membrane fluidity does not predict TREK-1 activation pressure. Mean membrane anisotropy and TREK-1 activation pressure were plotted. Pearson's r in (D-F) was determined to measure correlation strength, error bars represent standard error of the mean, n > 10 for each measurement.

Discussion

Through a series of micropipette aspiration and patch-clamp electrophysiology studies, we have determined the effect of various poloxamers and a chemically-distinct detergent on membrane properties and mechanosensitive channel behavior. By measuring these properties directly, we found that membrane K_A and k_c correlate with activation sensitivity of a mechanosensitive MscL variant, while membrane fluidity does not to the same extent. We found that the amphiphiles we

used did not appear to change membrane thickness or occlude MscL pores, factors that would be expected to impact channel activity. Finally, we determined that K_A and k_c may also affect the behavior of more complex mechanosensitive channels in higher organisms by assessing the behavior of TREK-1 in response to changes in membrane properties. Our findings suggest that by decreasing membrane K_A and k_c, a greater force is required to activate MscL and TREK-1. To our knowledge, our study is the first to directly measure multiple membrane properties in conjunction with electrophysiology assessments to directly implicate K_A and k_c in MscL and TREK-1 activation sensitivity.

Mechanosensitive channel activation sensitivity is an important feature of all mechanosensitive channels. Overactive mechanosensitive channels may lead to deleterious effects ranging from a loss in cell volume in bacteria or red blood cells (Cahalan et al., 2015; Levin and Blount, 2004) to persistent itch disease in higher organisms (LaMotte, 2016). Membrane composition has been increasingly shown to modulate the force-from-lipids activation of mechanosensitive channels and this effect is hypothesized to be due to changes in global membrane properties (Bruno et al., 2007). We recently showed that membrane amphiphiles can impact membrane properties in unpredictable ways (Jacobs et al., 2021) underlying the importance of directly measuring membrane properties when drawing conclusions about their role in a physiological outcome. While a number of studies discuss the effects of membrane properties on mechanosensitive channel activation (Nomura et al., 2012; Ridone et al., 2018; Xue et al., 2020), few have directly measured membrane properties (Caires et al., 2017; Nakayama et al., 2018; Romero et al., 2019). Moreover, to the best of our knowledge no studies to date have used the classical micropipette aspiration technique (Kwok and Evans, 1981) in conjunction with patch-clamp electrophysiology to directly determine the relationship between membrane properties and mechanosensitive channel function. Accordingly, the body of research to date has left an unexplored gap between membrane mechanical properties and mechanosensitive channel behavior that we have sought to address. In the present study, we demonstrated that membrane elastic properties modulate the force-from-lipids activation of two mechanosensitive channels.

Although most poloxamers we studied exhibited a monotonic effect on membrane properties and channel activation as a function of poloxamer concentration, we observed a non-monotonic effect of P184 concentration on MscLG22S activation and k_c. While most poloxamers decreased K_A and k_c as a function of concentration (Figure 2, Figure 2-figure supplement 7, Figure 3-figure supplement 3), P184 induced a slight decrease in K_A at all concentrations while k_c decreased at low concentrations then increased at higher concentrations (Figure 3-figure supplement 3). Interestingly, we observed a similar effect between membrane k_c and MscLG22S activation pressure in the presence of P184. We found that MscLG22S activation pressure increased then decreased with increasing P184 concentration (Figure 3-figure supplement 2). This observation highlights that the influence of k_c may be stronger than K_A on MscLG22S activation for this particular polymer because k_c, but not K_A, correlated well with MscLG22S activation in the presence of P184. We are unsure of the mechanism of this non-monotonic effect of P184 on k_c but attribute it to the large number of hydrophobic blocks relative to the small number of hydrophilic blocks in the polymer which likely leads to the polymer residing in a different location in the membrane relative to the other polymers explored (Rabbel et al., 2015). For example, P184 may increase membrane stiffness at higher concentrations through interdigitation (Battaglia and Ryan, 2005) or through changing the depth of P184 insertion in the membrane at high concentrations which is known to alter membrane properties (Grage et al., 2022; Zaki and Carbone, 2017). This result suggests that the effect membrane amphiphiles have on membrane properties can vary as a function of not only amphiphile identity, but also concentration, and may affect membrane mechanical properties in unexpected, nonmonotonic ways, further underscoring

the importance of directly measuring membrane properties to determine their impact on a physiological response.

Our results highlight a potential role of K_A and k_c in MscL activation which is related to the lateral pressure profile. MscL is known to be sensitive to lateral pressure profile as demonstrated by activation upon insertion of LPC, a single-chain amphiphile with a large headgroup (Figure 1-figure supplement 8) (Bavi et al., 2014; Nomura et al., 2012). However, the membrane lateral pressure profile can only be estimated using simulations. As the lateral pressure profile directly relies on K_A and k_c (Zhan and Lazaridis, 2013), we were able to further assess the importance of the lateral pressure profile experimentally by measuring these parameters.

We expect that a lowered K_A and k_c reduce the pressure sensitivity of the explored mechanosensitive channels by better accommodating hydrophobic mismatch and decreasing lateral tension in the membrane upon application of negative pressure. First, as hydrophobic mismatch is one of the key activators of MscL (Ridone et al., 2018), our results may be explained by the ability of polymeric amphiphiles to support protein hydrophobic mismatch to a greater extent than natural lipids (Itel et al., 2015; Srinivas et al., 2005). Polymeric amphiphiles that decrease membrane K_A, and therefore enhance the membrane's ability to stretch, allow membranes under tension to remain thicker relative to polymer-free membranes (Zaki and Carbone, 2017). Because bilayer thinning is a major factor driving the threshold activation pressure of MscL, membranes that better sustain membrane thickness for a given applied tension should require more pressure to reach the bilayer thickness required to activate embedded MscL channels (Ridone et al., 2018). Second, the propagation of tension in a membrane is related to the membrane stretch modulus (Cohen and Shi, 2020). Accordingly, one mechanism that can explain our observations of decreased channel sensitivity observed across all the amphiphiles we measured, is that the polymers decreased the area expansion modulus, K_A, and correspondingly decreased membrane tension that results from a given, applied, negative pressure (Steinhardt et al., 2000). Such a mechanism is supported by previous findings which demonstrated that mechanosensitive channel activation is increased (requires less applied pressure) by amphiphiles which increase membrane tension (Cordero-Morales and Vásquez, 2018; Kloda et al., 2007). Together, our results suggest a mechanism where various poloxamers and $C_{12}E_8$ alter MscLG22S function through alteration of membrane elastic properties.

Finally, our observations of poloxamers interacting with membranes and altering mechanical properties and mechanosensitive channel activity highlight a potential unwanted effect of membrane amphiphiles on cellular membranes. Poloxamers represent a widely used class of nanoplastics. The concentrations of poloxamer we chose to assess in the present study are commonly used in laboratory cell culture applications to prevent cell sticking and improve cell integrity and are also found at these concentrations in household products (Guzniczak et al., 2018). Our findings suggest that poloxamers used at these concentrations may alter the behavior of membrane-embedded ion channels which in turn may affect environmental and human health or may affect biophysical studies in unexplored ways. In addition, these findings propose one potential mechanism for the alteration of biological function in response to nanoplastic pollution which has remained elusive (Fleury and Baulin, 2021)—modulation of global membrane mechanical properties. Our results suggest that nanoplastics which have been increasingly shown to interact with cellular membranes (Fleury and Baulin, 2021; Goodman et al., 2021; Hollóczki and Gehrke, 2019), may alter biological function by modulating membrane physical properties and the subsequent behavior of membrane-embedded proteins (Huang et al., 2022; Ohashi et al., 2020).

Conclusion

In conclusion, we observed that various membrane-associating amphiphiles that decrease two membrane mechanical properties—membrane K_A and k_c—increase the force required to activate mechanosensitive channels. Our study is the first to our knowledge to measure mechanosensitive channel activation altered through membrane-associating polymers. By harnessing the unique features of polymeric amphiphiles, we probed the relationship between membrane K_A, k_c, fluidity, and mechanosensitive channel activation while maintaining membrane thickness. These observations, using two distinct mechanosensitive channels, highlight a direct connection between the membrane physical environment and mechanosensitive function to show that K_A and k_c are important drivers of mechanical force to ion channels. This finding suggests that as membranes become more elastic and can more easily accommodate applied tension through increases in membrane stretching and bending, they transmit less force to embedded mechanosensitive channels. As a result, higher applied forces are required to activate the channel that resides in such an environment. Our results, accordingly, support the force-from-lipids mechanism of mechanosensitive channel activation by demonstrating that membrane composition and the associated bilayer mechanical properties can modulate mechanosensitive function through long-range, indirect interactions.

Acknowledgements
This study was supported by the Air Force Office of Scientific Research YIP (FA9550-19-1-0039 P00001 to NPK) and the National Science Foundation (DMR-2145050 to NPK). This work was funded in part by the Chicago Biomedical Consortium with support from the Searle Funds at The Chicago Community Trust (to NPK and SMC). The authors acknowledge partial support from NIA/NINDS, National Institutes of Health (R01NS114413 to SMC) and the Department of Chemistry, College of Liberal Arts and Sciences, University of Illinois Chicago. MLJ was supported by Grant No. T32GM008382 from the National Institute of General Medical Sciences and the American Heart Association Predoctoral Fellowship under Grant No. 20PRE35180215. MJL was supported by NU's Molecular Biophysics Training Program through NIH NIGMS (5T32 GM008382). PGD was supported by NIH NIDDK (1R56DK119709-01, 1R01DK123463-01). This research was supported in part through the computational resources and staff contributions provided for the Quest high performance computing facility at Northwestern University which is jointly supported by the Office of the Provost, the Office for Research, and Northwestern University Information Technology.

Material and Methods

Materials

Gibco G418 (geneticin), McCoy's 5A medium, Opti-MEM transfection medium, Fetal Bovine Serum (FBS), $CaCl_2$, MES sodium salt, BAPTA NA_4 Poloxamer 188, 124, and 184, diphenylhexatriene, and polyethylenimine were obtained from Thermo Fisher Scientific. HEPES, NaCl, N-ethylmaleimide, and EGTA was purchased from Millipore Sigma. Human Osteosarcoma U-2 OS HTB-96 cell line was purchased from ATCC.

Methods

Mammalian expression plasmid cloning

EcMscLGFP was amplified using polymerase chain reaction (PCR) and inserted into a mammalian pCDNA3.0 vector using restriction digest. A G22C mutation was introduced in the *mscl* gene using primers with a point mutation and the entire plasmid was amplified using PCR. The cloned plasmids were transformed into Top10 electrocompetent cells and amplified and functional gene insertion was verified using sanger sequencing. TREK-1 was amplified with using

PCR and cloned into the pCDNA3.0 vector as a fusion to GFP by removal of EcMscL using restriction enzymes. Insertion and GFP fusion of TREK-1 was confirmed using sanger sequencing. pET19b:EcMscLGFP was used previously as an *in vitro* membrane protein folding reporter (Addgene plasmid # 165097) (Jacobs et al., 2019). pGEMHE:mTREK-1(K271Q) was a gift from Dan Minor (Addgene plasmid # 133270) (Lolicato et al., 2017).

Stable cell line transfection and selection

U2OS cells were plated in a 6-well plate and grown to 70% confluency on the day of transfection. Mammalian expression vectors containing EcMscLGFP or TREK-1GFP were transfected into U2OS cells using polyethylenimine (PEI). 500 ng DNA was mixed with 100 μL Opti-MEM transfection media and 2.5 μg PEI. This solution was incubated for 15 minutes then added dropwise to U2OS cells in McCoy's 5A media with 10% FBS. The transfection media was replaced with fresh McCoy's 5A with 10% FBS and 300 μg/mL geneticin after overnight incubation. Transfected cells were selected using 300 μg/mL geneticin in McCoy's 5A media with 10% FBS for 1 month or until the cells reached confluency in a T-75 75 cm^2 flask. Cells were further propagated in McCoy's 5A with 10% FBS and 100 μg/mL geneticin. Selection efficiency was confirmed using the GFP tag attached to the protein of interest.

GPMV formation and treatment with poloxamer

GPMV formation was performed using established techniques (Sezgin et al., 2012). Briefly, U2OS cells were plated at least one day prior to GPMV formation and grown to 70% confluency at the time of GPMV formation. GPMV buffer was used for all GPMV preparations and consisted of 10 mM HEPES, pH 7.4, 150 mM NaCl, and 2 mM $CaCl_2$. N-ethylmaleimide (NEM) was prepared at 0.25 M in sterile water and stored in 300 μL aliquots. 30 μL NEM was added to 1 mL of GPMV buffer containing the indicated concentration of pre-dissolved poloxamer or detergent and mixed using a vortex. Cells were washed twice with GPMV buffer and removed by aspiration. The NEM-GPMV buffer solution was added gently to the U2OS cells and incubated at 37 °C for 1 hour. GPMVs were observed then removed from adherent cells by gentle aspiration and were incubated for 3 hours at 4 °C prior to experiments to ensure poloxamer equilibration.

Fluorescence and phase-contrast microscopy

Cells and GPMVs were imaged using epifluorescence and phase-contrast microscopy to confirm transfection and protein transfer to GPMV membranes. Glass bottom 96-well plates were passivated by incubating β-casein solution at 5 mg/mL in 10 mM Tris, pH 7.4 in each well for 30 minutes. This solution was replaced with GPMV buffer, pH 7.4 and GPMVs were diluted to a concentration suitable to observe single GPMVs. GPMV area was images using differential interference contrast (DIC) phase contrast and Transfection efficiency and membrane protein integration were confirmed using epifluorescence with a GFP filter. All images being compared were brightness/contrast adjusted with identical settings and imaged at 20% light with identical exposure times.

Micropipette aspiration

GPMV membrane area expansion modulus (K_A) and bending rigidity (k_c) were measured using micropipette aspiration techniques (Evans et al., 1976). Micropipettes were constructed from borosilicate glass capillaries (World Precision Instruments) pulled using a P-1000 micropipette puller (Sutter instruments). The end was blunted and polished to an inner diameter of 5–8 *μ*m using a microforge. The micropipette and sample chamber surfaces were passivated using 5 mg/mL β-casein for 1 hour and were filled with GPMV buffer, pH 7.4. 10 μL GPMVs prepared in the presence of poloxamer or detergent were diluted in a 1 mL glass chamber in GPMV buffer, pH 7.4 (10 mM HEPES, 150 mM NaCl, 2 mM $CaCl_2$). Imaging was performed on a Nikon inverted

microscope connected to a Validyne pressure sensor and digital manometer (model DP 15-32; Validyne Engineering, Northridge, CA). A Narishige micromanipulator was used to control the micropipette (model WR-6; Narishige). GPMVs free of visible defects were aspirated and the membrane areal response to a change in pressure was measured using a series of DIC images with pressure recordings. Membrane K_{app} is calculated from the slope of the percent area dilation within the pipette ($\Delta A/A_o$) and membrane tension (τ),

$$K_{app} = \frac{\tau}{\frac{\Delta A}{A_o}}$$

where ΔA is the change in area of GPMV membrane within the micropipette and A_o is the initial area of the aspirated GPMV within the pipette. Compared to previous studies K_{app} was measured at elevated tensions that recruit any membrane area reservoirs and thus probe the elastic response of the membrane (Steinkühler et al., 2021). Bending elastic modulus, k_c is calculated from the same aspiration measurements through the following equation in the low-tension regime (<0.5 mN/m),

$$\frac{\ln(\tau)}{\frac{\Delta A}{A_o}} = \frac{8\pi k_c}{k_B T}$$

where k_B is the Boltzmann constant, and T is temperature. Membrane K_A is calculated through correction of K_{app} with k_c by subtraction for relaxation of thermal undulations measured by k_c (Rawicz et al., 2000; Zhou and Raphael, 2005). For each stress/strain measurement in the area expansion regime, the contributions of thermal undulations ($\Delta\alpha(i)$) was subtracted from the areal strain ($\Delta A/A_o$),

$$\Delta\alpha(i) = \frac{k_B T}{8\pi k_c} \ln\left(\frac{\tau(i)}{\tau(1)}\right)$$

where $\tau(1)$ is the initial tension. The corrected areal change was then plotted against τ and the slope of this plot was used to calculate K_A.

Patch Clamp electrophysiology of stretch-activated ion channels

Channel activity measurements were performed in identical conditions as micropipette aspiration. GPMVs containing EcMscL and TREK-1 prepared under indicated poloxamer conditions were added to an open-air bath on an Olympus IX73 phase-contrast microscope. Electrophysiology pipettes were pulled using a Sutter P-1000 micropipette puller and fire polished using a microforge to 5-8 MΩ resistance. Voltage-clamp measurements were recorded on a Molecular Devices Axon Instruments system including an amplifier and digitizer Low-Noise Data Acquisition System plus Hum silencer along with an ALA Scientific Instruments High Speed Pressure Clamp pressure controller which was used to apply a pressure ramp during electrophysiology recordings. All signals were integrated using Clampex software and pressure and current values were recorded temporally. A pressure ramp from 0 mmHg to -160 mmHg was applied at a constant rate for all recordings. EcMscL and TREK-1 recordings were performed at -10 mV and -40 mV, respectively unless channel conductance calculations were being measured. Current and pressure were recorded through these experiments using and were used to calculate pressure sensitivity and channel conductance, respectively. Each pressure sensitivity recording was performed on an independent GPMV and pressure ramps were never repeated as a decrease in pressure sensitivity is observed after repeat pressure ramps because of an increase in membrane tension when the membrane patch diffuses up the pipette (Nomura et al., 2012). All electrophysiology recordings were performed at 25 °C Bath solution was composed of 10 mM HEPES, pH 7.4, 150 mM NaCl, 2 mM $CaCl_2$ for MscL and 10 mM HEPES, pH 7.4, 150 mM KCl, 2 mM $CaCl_2$ for TREK-1. The pipette solution was composed of 10 mM HEPES, pH 7.4, 100 mM NaMES, 10 mM BAPTA Na_4, 10 mM NaCl, 10 mM EGTA. All recordings were performed in the cell-attached or excised-

patch configuration. A seal > 8 GΩ was used as criteria for analysis of single-channel observations.

Electrophysiology data analysis

Electrophysiology experiments were quantified using Clampfit software which displayed the current and pressure during the voltage-clamp recording. EcMscL and TREK-1 channel activation sensitives were quantified using the pressure at first channel opening which has been described previously (Nomura et al., 2012). Many recordings only contained one channel, and this first channel was clearly distinguished from electrical noise. However, some recordings contained many channels which could not be distinguished from membrane unsealing making maximum current an unreliable measurement. Membrane rupture pressure was calculated by the pressure at which a very large current change occurred, indicating complete membrane rupture. Single channel conductance was measured by calculating the current through single channels at various voltages and was independent from pipette pressure. Each current and voltage measurement was recorded from an independent GPMV, and this measurement was not repeated by any single GPMV to mimic pressure sensitivity measurement conditions. The slope of many of these I/V relationships was used to calculate channel conductance. TREK-1 was observed to behave similarly to previous studies and had a short dwell time and was potassium selective with a much smaller conductance than MscL (Xian Tao Li et al., 2006).

Mass Spectrometry

Mass spectrometry (MS) was used to characterize the integration of poloxamer into the GPMVs. Samples were prepared as described for GPMV formation and free poloxamer was removed by centrifugation. Pelleted GPMVs were stored at -80 °C until analysis. Matrix-assisted laser desorption/ionization time of flight (MALDI-TOF) MS was carried out using an Autoflex® speed MALDI-TOF (Bruker Daltonik GmbH,Bremen Germany) A 10 mg/mL matrix solution of α-cyano-4-hydroxycinnamic acid (CHCA) in 70% ACN in water with 0.1% trifluoroacetic acid (TFA) was prepared. Using the dried drop (DD) method, aqueous solutions of P124-only, P188-only standards and P124-GMPV, P188-GMPV integrated samples were mixed with the matrix at a ratio of 1:1 (vol/vol). For each sample, 5000 shots were fired using the “random walk” function. Positive ion data was collected in both the linear and reflectron modes with external calibration. The acquisition mass ranges were *m/z* 1000–4000 and *m/z* 4000–12500 for P124 samples and P188 samples, respectively. For the poloxamer(P)-GMPV samples, mass range for the P-GMPV lipids was *m/z* 500–1000.

Anisotropy

Fluorescence anisotropy measurements were used to determine relative membrane fluidity as described previously (Jacobs et al., 2021). GPMVs were prepared and unbound poloxamer micelles were removed from solution through centrifugation and GPMVs were rehydrated in 1 mL GPMV buffer. A diphenylhexatriene (DPH) stock solution was prepared by adding dry DPH to GPMV buffer at 100 μM. This solution was mixed 1:1 with purified GPMVs and anisotropy was measured using an Agilent Technologies Cary Eclipse Fluorescence Spectrophotometer with an Automated Polarization Accessory. Fluorescence anisotropy was assessed at excitation 360 nm and emission 435 nm and was calculated by software provided with the instrument,

$$\text{anisotropy} = \frac{I_{vv} - I_{vh}G}{I_{vv} + 2I_{vh}G}$$

where I_{vv} and I_{vh} are the intensities of the vertically and horizontally polarized light, respectively, after excitation with vertically polarized light. $G = I_{hv}/I_{hh}$ which is a grating correction factor for the optical system.

Chemical activation of MscL and calcium imaging

Fluo4, a calcium indicator which has been used previously to sense mechanosensitive channel behavior (Cahalan et al., 2015), was used to determine if P124 inhibits MscL activation through inhibition of pore hydration. Briefly, Fluo4 was mixed with GPMV buffer to a 1x dye concentration. GPMV formation solution was prepared by adding 30 μL of 0.25 M NEM to 1 mL of diluted Fluo4 solution in GPMV buffer. Cells were washed twice with GPMV buffer and incubated in GPMV formation solution for 1 hour at 37 °C. Free-floating GPMVs were isolated by transferring formation solution to an Eppendorf tube and incubated for 3 additional hours. A glass-bottom 96-well plate was passivated by incubating with a β-casein solution in 10 mM Tris, pH 7.4 for 30 min. The wells were rinsed 3 times with GPMV buffer and 100 μL GPMV buffer with 5 mM $CaCl_2$ was added to each desired well. 10 μL GPMVs were added to the bottom of each well. 5 μL of 21 mM MTSET was added to each well and GPMVs were incubated for 30 min. Ca^{2+} influx through MscL opening was quantified from raw images by a fluorescence increase in the GFP channel for each GPMV visible in the DIC channel.

Molecular Dynamics Simulations

PL124 polymer was assembled using CHARMM-GUI Polymer Builder from PEO and PPO groups from the CHARMM36 forcefield (Choi et al., 2021; Jo et al., 2008). Based on previous work (Rabbel et al., 2015) we assumed that P124 inserts as a harpin into the membrane. We further assumed that the incubation time is sufficient for P124 to flip-flop in the membrane and assume a symmetric configuration. The polymer chains were pre-equilibrated in water and a harpin-like conformation was selected by hand. The appropriate number polymer chain copies were then inserted to a pre-equilibrated DOPC membrane (300 lipids in total). The parallel periodic membrane images were separated by a 4 nm water layer. Simulations were run using GROMACS (2020) with a timestep of 2 fs, Verlet cutoff-scheme, electrostatics and LJ interactions cutoff at 1.2 nm and PME long-range electrostatics. Simulations were run NPT ensemble, using a Nose-Hoover thermostat and semi-isotropic Parrinello-Rahman pressure coupling for a (laterally) tensionless membrane. Temperature coupling was done with the Nose-Hoover algorithm. The membrane elastic modulus K_A was estimated from the thermal bilayer lateral area fluctuations from a (fully equilibrated) 500 ns long trajectory (Feller and Pastor, 1999). Membrane thickness was calculated from the lipid headgroup phosphate distances between the two leaflets using MDAnalysis version 0.20.1 (Michaud-Agrawal et al., 2011). Statistical uncertainties in the membrane elastic modulus and thickness were estimated using blocking analysis (Flyvbjerg and Petersen, 1989) implemented in pyblock (James Spencer, http://github.com/jsspencer/pyblock) with block sizes chosen to remove temporal correlation from the data set (Wolff, 2004).

References

Anishkin A, Loukin SH, Teng J, Kung C. 2014. Feeling the hidden mechanical forces in lipid bilayer is an original sense. *Proc Natl Acad Sci* **111**:7898–7905. doi:10.1073/pnas.1313364111

Balleza D. 2012. Mechanical properties of lipid bilayers and regulation of mechanosensitive function: From biological to biomimetic channels. *Channels* **6**:220–233. doi:10.4161/chan.21085

Banerjee A, Lee A, Campbell E, MacKinnon R. 2013. Structure of a pore-blocking toxin in complex with a eukaryotic voltage-dependent K+ channel. *Elife* **2013**:1–22. doi:10.7554/eLife.00594

Battaglia G, Ryan AJ. 2005. Bilayers and interdigitation in block copolymer vesicles. *J Am Chem Soc* **127**:8757–8764. doi:10.1021/ja050742y

Bavi O, Vossoughi M, Naghdabadi R, Jamali Y. 2014. The effect of local bending on gating of MscL using a representative volume element and finite element simulation. *Channels* **8**:344–349. doi:10.4161/chan.29572

Brohawn SG, Su Z, MacKinnon R. 2014. Mechanosensitivity is mediated directly by the lipid membrane in TRAAK and TREK1 K^+ channels. *Proc Natl Acad Sci* **111**:3614–3619. doi:10.1073/pnas.1320768111

Brohawn SG, Wang W, Handler A, Campbell EB, Schwarz JR, MacKinnon R. 2019. The mechanosensitive ion channel TRAAK is localized to the mammalian node of Ranvier. *Elife* **8**:1–22. doi:10.7554/eLife.50403

Bruno MJ, Koeppe RE, Andersen OS. 2007. Docosahexaenoic acid alters bilayer elastic properties. *Proc Natl Acad Sci* **104**:9638–9643. doi:10.1073/pnas.0701015104

Cahalan SM, Lukacs V, Ranade SS, Chien S, Bandell M, Patapoutian A. 2015. Piezo1 links mechanical forces to red blood cell volume. *Elife* **4**. doi:10.7554/eLife.07370

Caires R, Sierra-Valdez FJ, Millet JRM, Herwig JD, Roan E, Vásquez V, Cordero-Morales JF. 2017. Omega-3 Fatty Acids Modulate TRPV4 Function through Plasma Membrane Remodeling. *Cell Rep* **21**:246–258. doi:10.1016/j.celrep.2017.09.029

Calori IR, Pinheiro L, Braga G, Morais FAP de, Caetano W, Tedesco AC, Hioka N. 2022. Interaction of triblock copolymers (Pluronics®) with DMPC vesicles: a photophysical and computational study. *Spectrochim Acta Part A Mol Biomol Spectrosc* 121178. doi:10.1016/j.saa.2022.121178

Chang G, Spencer RH, Lee AT, Barclay MT, Rees DC. 1998. Structure of the MscL homolog from Mycobacterium tuberculosis: A gated mechanosensitive ion channel. *Science (80-)* **282**:2220–2226. doi:10.1126/science.282.5397.2220

Choi YK, Park SJ, Park S, Kim S, Kern NR, Lee J, Im W. 2021. CHARMM-GUI Polymer Builder for Modeling and Simulation of Synthetic Polymers. *J Chem Theory Comput* **17**:2431–2443. doi:10.1021/acs.jctc.1c00169

Cohen AE, Shi Z. 2020. Do Cell Membranes Flow Like Honey or Jiggle Like Jello? *BioEssays* **42**:1–13. doi:10.1002/bies.201900142

Cordero-Morales JF, Vásquez V. 2018. How lipids contribute to ion channel function, a fat perspective on direct and indirect interactions. *Curr Opin Struct Biol* **51**:92–98. doi:10.1016/j.sbi.2018.03.015

Cox CD, Bavi N, Martinac B. 2019. Biophysical Principles of Ion-Channel-Mediated Mechanosensory Transduction. *Cell Rep* **29**:1–12. doi:10.1016/j.celrep.2019.08.075

Dave N, Cetiner U, Arroyo D, Fonbuena J, Tiwari M, Barrera P, Lander N, Anishkin A, Sukharev S, Jimenez V. 2021. A novel mechanosensitive channel controls osmoregulation, differentiation, and infectivity in trypanosoma cruzi. *Elife* **10**:1–32. doi:10.7554/ELIFE.67449

del Mármol JI, Touhara KK, Croft G, MacKinnon R. 2018. Piezo1 forms a slowly-inactivating mechanosensory channel in mouse embryonic stem cells. *Elife* **7**:1–18. doi:10.7554/eLife.33149

Doerner JF, Febvay S, Clapham DE. 2012. Controlled delivery of bioactive molecules into live cells using the bacterial mechanosensitive channel MscL. *Nat Commun* **3**:990. doi:10.1038/ncomms1999

Evans EA, Waugh R, Melnik L. 1976. Elastic area compressibility modulus of red cell membrane. *Biophys J* **16**:585–595. doi:10.1016/S0006-3495(76)85713-X

Feller SE, Pastor RW. 1999. Constant surface tension simulations of lipid bilayers: The sensitivity of surface areas and compressibilities. *J Chem Phys* **111**:1281–1287. doi:10.1063/1.479313

Fleury JB, Baulin VA. 2021. Microplastics destabilize lipid membranes by mechanical stretching. *Proc Natl Acad Sci U S A* **118**:1–8. doi:10.1073/pnas.2104610118

Flyvbjerg H, Petersen HG. 1989. Error estimates on averages of correlated data. *J Chem Phys* **91**:461–466. doi:10.1063/1.457480

Goodman KE, Hare JT, Khamis ZI, Hua T, Sang QXA. 2021. Exposure of Human Lung Cells to Polystyrene Microplastics Significantly Retards Cell Proliferation and Triggers Morphological Changes. *Chem Res Toxicol* **34**:1069–1081. doi:10.1021/acs.chemrestox.0c00486

Grage SL, Afonin S, Ieronimo M, Berditsch M, Wadhwani P, Ulrich AS. 2022. Probing and Manipulating the Lateral Pressure Profile in Lipid Bilayers Using Membrane-Active Peptides—A Solid-State 19F NMR Study. *Int J Mol Sci* **23**:4544. doi:10.3390/ijms23094544

Großkopf S, Fouquet P, Wiehemeier L, Hellweg T. 2021. Pluronic-based lamellar phases: influence of polymer architecture on bilayer bending elasticity. *Mol Phys* **119**. doi:10.1080/00268976.2021.1893400

Guo YR, MacKinnon R. 2017. Structure-based membrane dome mechanism for piezo mechanosensitivity. *Elife* **6**:1–19. doi:10.7554/eLife.33660

Guzniczak E, Jimenez M, Irwin M, Otto O, Willoughby N, Bridle H. 2018. Impact of poloxamer 188 (Pluronic F-68) additive on cell mechanical properties, quantification by real-time deformability cytometry. *Biomicrofluidics* **12**:044118. doi:10.1063/1.5040316

Heureaux J, Chen D, Murray VL, Deng CX, Liu AP. 2014. Activation of a Bacterial Mechanosensitive Channel in Mammalian Cells by Cytoskeletal Stress. *Cell Mol Bioeng* **7**:307–319. doi:10.1007/s12195-014-0337-8

Heurteaux C, Guy N, Laigle C, Blondeau N, Duprat F, Mazzuca M, Lang-Lazdunski L, Widmann C, Zanzouri M, Romey G, Lazdunski M. 2004. TREK-1, a K+ channel involved in neuroprotection and general anesthesia. *EMBO J* **23**:2684–2695. doi:10.1038/sj.emboj.7600234

Hollóczki O, Gehrke S. 2019. Can Nanoplastics Alter Cell Membranes? *ChemPhysChem* 9–12. doi:10.1002/cphc.201900481

Houk AR, Jilkine A, Mejean CO, Boltyanskiy R, Dufresne ER, Angenent SB, Altschuler SJ, Wu LF, Weiner OD. 2012. Membrane tension maintains cell polarity by confining signals to the leading edge during neutrophil migration. *Cell* **148**:175–188. doi:10.1016/j.cell.2011.10.050

Huang SK, Almurad O, Pejana RJ, Morrison ZA, Pandey A, Picard LP, Nitz M, Sljoka A, Prosser RS. 2022. Allosteric modulation of the adenosine A2A receptor by cholesterol. *Elife* **11**:1–24. doi:10.7554/ELIFE.73901

Itel F, Najer A, Palivan CG, Meier W. 2015. Dynamics of Membrane Proteins within Synthetic Polymer Membranes with Large Hydrophobic Mismatch. *Nano Lett* **15**:3871–3878. doi:10.1021/acs.nanolett.5b00699

Jacobs ML, Boyd MA, Kamat NP. 2019. Diblock copolymers enhance folding of a mechanosensitive membrane protein during cell-free expression. *Proc Natl Acad Sci* **116**:4031–4036. doi:10.1073/pnas.1814775116

Jacobs ML, Faizi HA, Peruzzi JA, Vlahovska PM, Kamat NP. 2021. EPA and DHA differentially modulate membrane elasticity in the presence of cholesterol. *Biophys J* **120**:2317–2329. doi:10.1016/j.bpj.2021.04.009

Jo S, Kim T, Iyer GV, Im W. 2008. CHARMM-GUI: A Web-Based Graphical User Interface for CHARMM. *J Comput Chem* **29**:1859–1865. doi:10.1002/jcc

Johnson SL. 2015. Membrane properties specialize mammalian inner hair cells for frequency or intensity encoding. *Elife* **4**:1–21. doi:10.7554/elife.08177

Keller H, Lorizate M, Schwille P. 2009. PI(4,5)P2 Degradation Promotes the Formation of Cytoskeleton-Free Model Membrane Systems. *ChemPhysChem* **10**:2805–2812. doi:10.1002/cphc.200900598

Kloda A, Lua L, Hall R, Adams DJ, Martinac B. 2007. Liposome reconstitution and modulation of recombinant N-methyl-D-aspartate receptor channels by membrane stretch. *Proc Natl Acad Sci U S A* **104**:1540–1545. doi:10.1073/pnas.0609649104

Kwok R, Evans E. 1981. Thermoelasticity of large lecithin bilayer vesicles. *Biophys J* **35**:637–652. doi:10.1016/S0006-3495(81)84817-5

Lacampagne A, Gannier F, Argibay J, Garnier D, Le Guennec JY. 1994. The stretch-activated ion channel blocker gadolinium also blocks L-type calcium channels in isolated ventricular myocytes of the guinea-pig. *BBA - Biomembr* **1191**:205–208. doi:10.1016/0005-2736(94)90250-X

LaMotte RH. 2016. Allergic Contact Dermatitis: A Model of Inflammatory Itch and Pain in Human and Mouse In: Ma C, Huang Y, editors. Translational Research in Pain and Itch. Dordrecht: Springer Netherlands. pp. 23–32. doi:10.1007/978-94-017-7537-3_2

Levental KR, Lorent JH, Lin X, Skinkle AD, Surma MA, Stockenbojer EA, Gorfe AA, Levental I. 2016. Polyunsaturated lipids regulate membrane domain stability by tuning membrane order. *Biophys J* **110**:1800–1810. doi:10.1016/j.bpj.2016.03.012

Levin G, Blount P. 2004. Cysteine Scanning of MscL Transmembrane Domains Reveals Residues Critical for Mechanosensitive Channel Gating. *Biophys J* **86**:2862–2870. doi:10.1016/S0006-3495(04)74338-6

Lolicato M, Arrigoni C, Mori T, Sekioka Y, Bryant C, Clark KA, Minor DL. 2017. K2P2.1 (TREK-1)–activator complexes reveal a cryptic selectivity filter binding site. *Nature* **547**:364–368. doi:10.1038/nature22988

Lundbæk JA, Birn P, Hansen AJ, Søgaard R, Nielsen C, Girshman J, Bruno MJ, Tape SE, Egebjerg J, Greathouse D V, Mattice GL, Koeppe RE, Andersen OS. 2004. Regulation of Sodium Channel Function by Bilayer Elasticity: The Importance of Hydrophobic Coupling. Effects of Micelle-forming Amphiphiles and Cholesterol. *J Gen Physiol* **123**:599–621. doi:10.1085/jgp.200308996

Lundbæk JA, Collingwood SA, Ingólfsson HI, Kapoor R, Andersen OS. 2010. Lipid bilayer regulation of membrane protein function: gramicidin channels as molecular force probes. *J R Soc Interface* **7**:373–395. doi:10.1098/rsif.2009.0443

Martinac B, Nikolaev YA, Silvani G, Bavi N, Romanov V, Nakayama Y, Martinac AD, Rohde P, Bavi O, Cox CD. 2020. Cell membrane mechanics and mechanosensory transduction, 1st ed, Current Topics in Membranes. Elsevier Inc. doi:10.1016/bs.ctm.2020.08.002

Michaud-Agrawal N, Denning EJ, Woolf TB, Beckstein O. 2011. MDAnalysis: A toolkit for the analysis of molecular dynamics simulations. *J Comput Chem* **32**:2319–2327. doi:10.1002/jcc.21787

Nakayama Y, Komazawa K, Bavi N, Hashimoto K ichi, Kawasaki H, Martinac B. 2018. Evolutionary specialization of MscCG, an MscS-like mechanosensitive channel, in amino acid transport in Corynebacterium glutamicum. *Sci Rep* **8**:1–13. doi:10.1038/s41598-018-31219-6

Nomura T, Cranfield CG, Deplazes E, Owen DM, Macmillan A, Battle AR, Constantine M, Sokabe M, Martinac B. 2012. Differential effects of lipids and lyso-lipids on the

mechanosensitivity of the mechanosensitive channels MscL and MscS. *Proc Natl Acad Sci* **109**:8770–8775. doi:10.1073/pnas.1200051109
Ohashi Y, Tremel S, Masson GR, McGinney L, Boulanger J, Rostislavleva K, Johnson CM, Niewczas I, Clark J, Williams RL. 2020. Membrane characteristics tune activities of endosomal and autophagic human VPS34 complexes. *Elife* **9**:1–28. doi:10.7554/eLife.58281
Otten D, Brown MF, Beyer K. 2000. Softening of Membrane Bilayers by Detergents Elucidated by Deuterium NMR Spectroscopy. *J Phys Chem B* **104**:12119–12129. doi:10.1021/jp001505e
Procko C, Murthy S, Keenan WT, Mousavi SAR, Dabi T, Coombs A, Procko E, Baird L, Patapoutian A, Chory J. 2021. Stretch-activated ion channels identified in the touch-sensitive structures of carnivorous droseraceae plants. *Elife* **10**:1–24. doi:10.7554/eLife.64250
Rabbel H, Werner M, Sommer JU. 2015. Interactions of Amphiphilic Triblock Copolymers with Lipid Membranes: Modes of Interaction and Effect on Permeability Examined by Generic Monte Carlo Simulations. *Macromolecules* **48**:4724–4732. doi:10.1021/acs.macromol.5b00720
Rawicz W, Olbrich KC, McIntosh T, Needham D, Evans E. 2000. Effect of Chain Length and Unsaturation on Elasticity of Lipid Bilayers. *Biophys J* **79**:328–339. doi:10.1016/S0006-3495(00)76295-3
Reddy B, Bavi N, Lu A, Park Y, Perozo E. 2019. Molecular basis of force-from-lipids gating in the mechanosensitive channel mscs. *Elife* **8**:1–24. doi:10.7554/eLife.50486
Ridone P, Grage SL, Patkunarajah A, Battle AR, Ulrich AS, Martinac B. 2018. “Force-from-lipids” gating of mechanosensitive channels modulated by PUFAs. *J Mech Behav Biomed Mater* **79**:158–167. doi:10.1016/j.jmbbm.2017.12.026
Ridone P, Pandzic E, Vassalli M, Cox CD, Macmillan A, Gottlieb PA, Martinac B. 2020. Disruption of membrane cholesterol organization impairs the activity of PIEZO1 channel clusters. *J Gen Physiol* **152**. doi:10.1085/jgp.201912515
Rokitskaya TI, Nazarov PA, Golovin A V., Antonenko YN. 2017. Blocking of Single α-Hemolysin Pore by Rhodamine Derivatives. *Biophys J* **112**:2327–2335. doi:10.1016/j.bpj.2017.04.041
Romero LO, Massey AE, Mata-Daboin AD, Sierra-Valdez FJ, Chauhan SC, Cordero-Morales JF, Vásquez V. 2019. Dietary fatty acids fine-tune Piezo1 mechanical response. *Nat Commun* **10**:1200. doi:10.1038/s41467-019-09055-7
Sezgin E, Kaiser HJ, Baumgart T, Schwille P, Simons K, Levental I. 2012. Elucidating membrane structure and protein behavior using giant plasma membrane vesicles. *Nat Protoc* **7**:1042–1051. doi:10.1038/nprot.2012.059
Shi Z, Innes-Gold S, Cohen AE. 2022. Membrane tension propagation couples axon growth and collateral branching. *bioRxiv* 2022.01.09.475560.
Srinivas G, Discher DE, Klein ML. 2005. Key roles for chain flexibility in block copolymer membranes that contain pores or make tubes. *Nano Lett* **5**:2343–2349. doi:10.1021/nl051515x
Steinhardt RA, Togo T, Krasieva TB. 2000. A Decrease in Membrane Tension Precedes Successful Cell-Membrane Repair. *Mol Biol Cell* **11**:4339–4346.
Steinkühler J, Fonda P, Bhatia T, Zhao Z, Leomil FSC, Lipowsky R, Dimova R. 2021. Superelasticity of Plasma- and Synthetic Membranes Resulting from Coupling of Membrane Asymmetry, Curvature, and Lipid Sorting. *Adv Sci* **8**:1–9. doi:10.1002/advs.202102109
Steinkühler J, Sezgin E, Urbančič I, Eggeling C, Dimova R. 2019. Mechanical properties of plasma membrane vesicles correlate with lipid order, viscosity and cell density. *Commun Biol* **2**:1–8. doi:10.1038/s42003-019-0583-3
Sukharev SI, Blount P, Martinac B, Blattnert FR, Kung C. 1994. A large-conductance

mechanosensitive channel in E. coli encoded by mscL alone. *Nature* **368**:265–268.
Sukharev SI, Sigurdson WJ, Kung C, Sachs F. 1999. Energetic and spatial parameters for gating of the bacterial large conductance mechanosensitive channel, MscL. *J Gen Physiol* **113**:525–539. doi:10.1085/jgp.113.4.525
Sun W, Chi S, Li Yuheng, Ling S, Tan Y, Xu Y, Jiang F, Li J, Liu C, Zhong G, Cao D, Jin X, Zhao D, Gao X, Liu Z, Xiao B, Li Yingxian. 2019. The mechanosensitive Piezo1 channel is required for bone formation. *Elife* **8**:1–25. doi:10.7554/eLife.47454
Teng J, Loukin S, Anishkin A, Kung C. 2015. The force-from-lipid (FFL) principle of mechanosensitivity, at large and in elements. *Pflügers Arch - Eur J Physiol* **467**:27–37. doi:10.1007/s00424-014-1530-2
Vásquez V, Krieg M, Lockhead D, Goodman MB. 2014. Phospholipids that Contain Polyunsaturated Fatty Acids Enhance Neuronal Cell Mechanics and Touch Sensation. *Cell Rep* **6**:70–80. doi:10.1016/j.celrep.2013.12.012
Wang Y, Guo Y, Li G, Liu C, Wang L, Zhang A, Yan Z, Song C. 2021. The push-to-open mechanism of the tethered mechanosensitive ion channel nompc. *Elife* **10**:1–20. doi:10.7554/eLife.58388
Wang Y, Liu Y, Deberg HA, Nomura T, Hoffman MT onks, Rohde PR, Schulten K, Martinac B, Selvin PR. 2014. Single molecule FRET reveals pore size and opening mechanism of a mechano-sensitive ion channel. *Elife* **3**:e01834. doi:10.7554/eLife.01834
Wolff U. 2004. Monte Carlo errors with less errors. *Comput Phys Commun* **156**:143–153. doi:10.1016/S0010-4655(03)00467-3
Xian Tao Li, Dyachenko V, Zuzarte M, Putzke C, Preisig-Müller R, Isenberg G, Daut J. 2006. The stretch-activated potassium channel TREK-1 in rat cardiac ventricular muscle. *Cardiovasc Res* **69**:86–97. doi:10.1016/j.cardiores.2005.08.018
Xue F, Cox CD, Bavi N, Rohde PR, Nakayama Y, Martinac B. 2020. Membrane stiffness is one of the key determinants of E. coli MscS channel mechanosensitivity. *Biochim Biophys Acta - Biomembr* **1862**:183203. doi:10.1016/j.bbamem.2020.183203
Yoshimura K, Batiza A, Kung C. 2001. Chemically Charging the Pore Constriction Opens the Mechanosensitive Channel MscL. *Biophys J* **80**:2198–2206. doi:10.1016/S0006-3495(01)76192-9
Zaki AM, Carbone P. 2017. How the Incorporation of Pluronic Block Copolymers Modulates the Response of Lipid Membranes to Mechanical Stress. *Langmuir* **33**:13284–13294. doi:10.1021/acs.langmuir.7b02244
Zhan H, Lazaridis T. 2013. Inclusion of lateral pressure/curvature stress effects in implicit membrane models. *Biophys J* **104**:643–654. doi:10.1016/j.bpj.2012.12.022
Zhou Y, Raphael RM. 2005. Effect of salicylate on the elasticity, bending stiffness, and strength of SOPC membranes. *Biophys J* **89**:1789–1801. doi:10.1529/biophysj.104.054510

Supplemental Figures

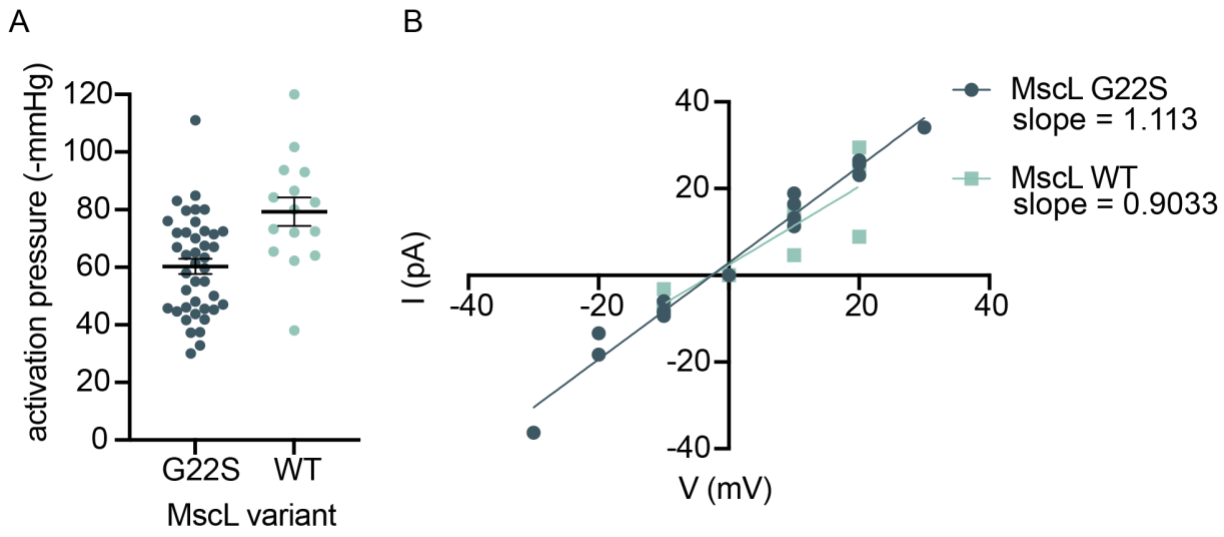

Figure 1–figure supplement 1

MscLG22S reduces the pressure required for activation compared to MscLWT but does not change channel conductance. A) MscL activation pressure is reduced in the G22S mutant. The pressure at first channel opening was measured to quantify MscL activation sensitivity. Individual points represent independent GPMV measurements. Mean is plotted with error bars which represent standard error of the mean. B) Conductance calculations for MScLG22S and MscLWT demonstrate that MscL channel size and selectivity is not affected by the G22S mutation. MscLG22S conductance = 1.113 nS (95% confidence interval 1.020 – 1.207). MscLWT conductance = 0.9033 nS (95% confidence interval 0.5761 – 1.231)

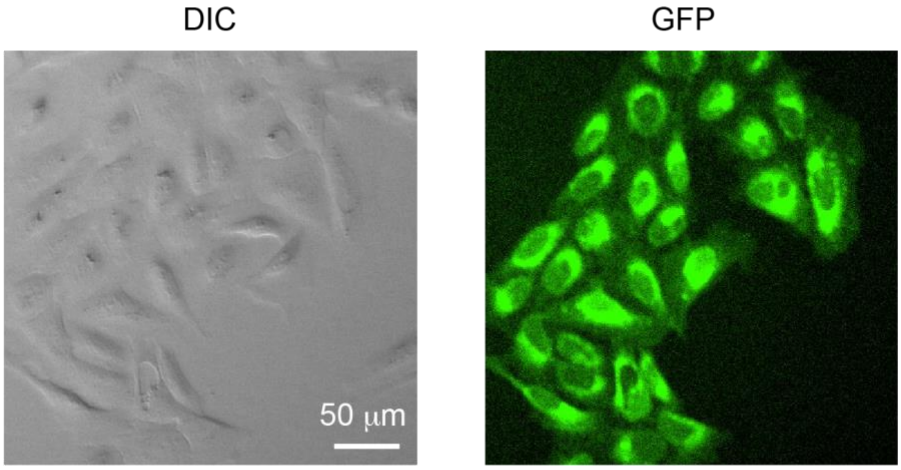

Figure 1–figure supplement 2

U2OS cell lines stably expressing MscLG22S tagged with GFP. MscLG22S expressed as a fusion protein with GFP was transfected into U2OS cells and selected using geneticin for 4 weeks. MscL is localized to various membranes within the cell including the plasma membrane.

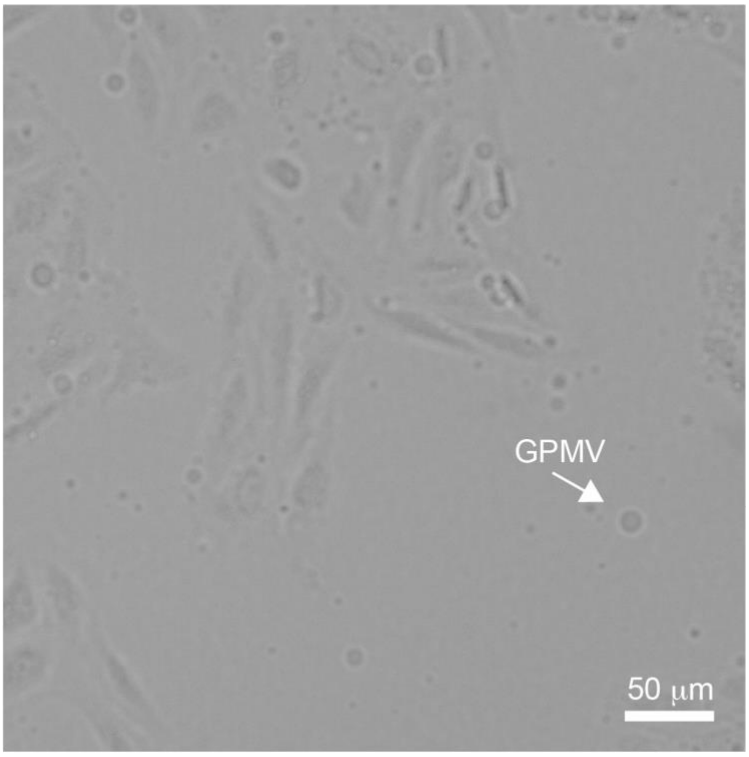

Figure 1–figure supplement 3

GPMVs budding off U2OS cells. DIC micrograph demonstrates Giant Plasma Membrane Vesicles (GPMVs) formation by budding off adherent mammalian cells. This process creates large diameter bilayer vesicles comprised of the cellular plasma membrane without cytoskeletal attachments or intracellular membranes.

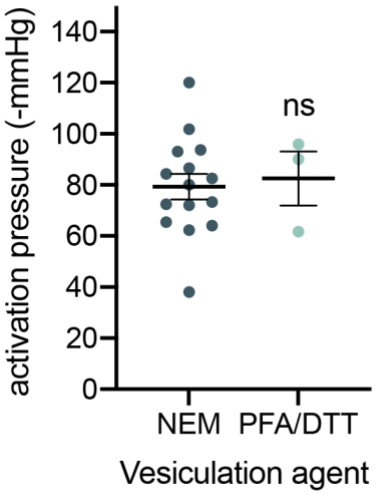

Figure 1–figure supplement 4

Differing GPMV formation methods yield similar MscL activation pressures, but crosslinking reagents reduce the probability of channel opening. GPMV formation is commonly performed using two different methods, NEM or PFA/DTT. While PFA/DTT is the most commonly used reagent mixture, this method induces crosslinking of lipids and proteins that is not amenable to mechanosensitive channel activation. In the presence of PFA/DTT, after >30 attempts over three independent GPMVs preparations, only three instances of MscL channels were observed. In contrast, NEM preparation allowed reliable observation of MscL activation. Both methods for GPMV formation did not demonstrate differing activation pressure thresholds of MscL. p-values to determine significance between means was measured using Student's t-test. non-significant (ns) $p > 0.05$, $n > 30$.

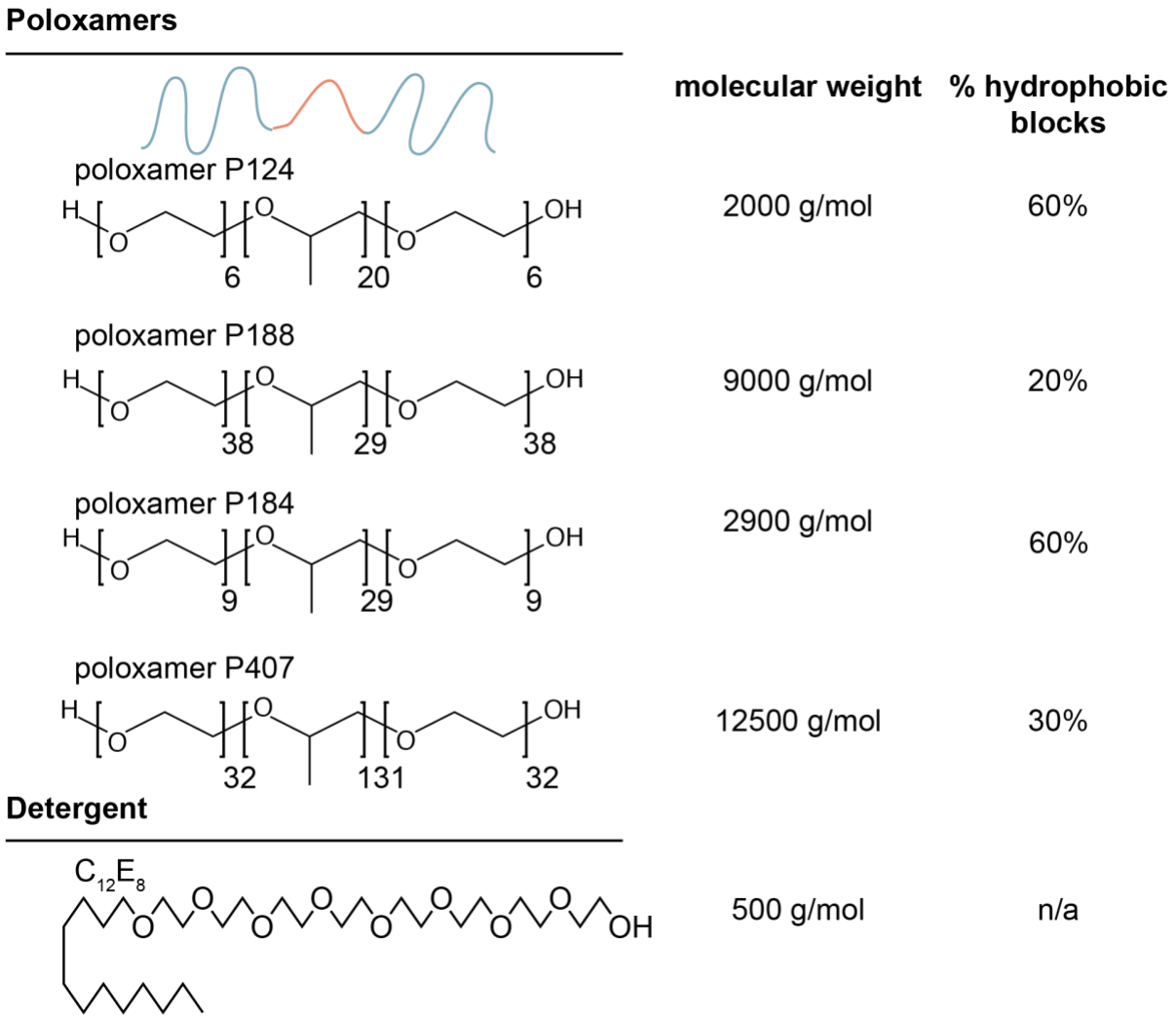

Figure 1–figure supplement 5

Schematic and properties of amphiphiles used in this study. We used various synthetic amphiphiles to exogenously alter membrane mechanical properties. These amphiphiles belong to two classes, poloxamer (Pluronic) and small nonionic detergent. Poloxamer is a class of triblock copolymers which consist of a polypropylene oxide hydrophobic block sandwiched by two polyethylene oxide hydrophilic blocks. Poloxamers have similar properties to surfactants in their ability to insert into bilayers but have much larger molecular weights. The detergent $C_{12}E_8$ we used has a much smaller molecular size in comparison to poloxamer.

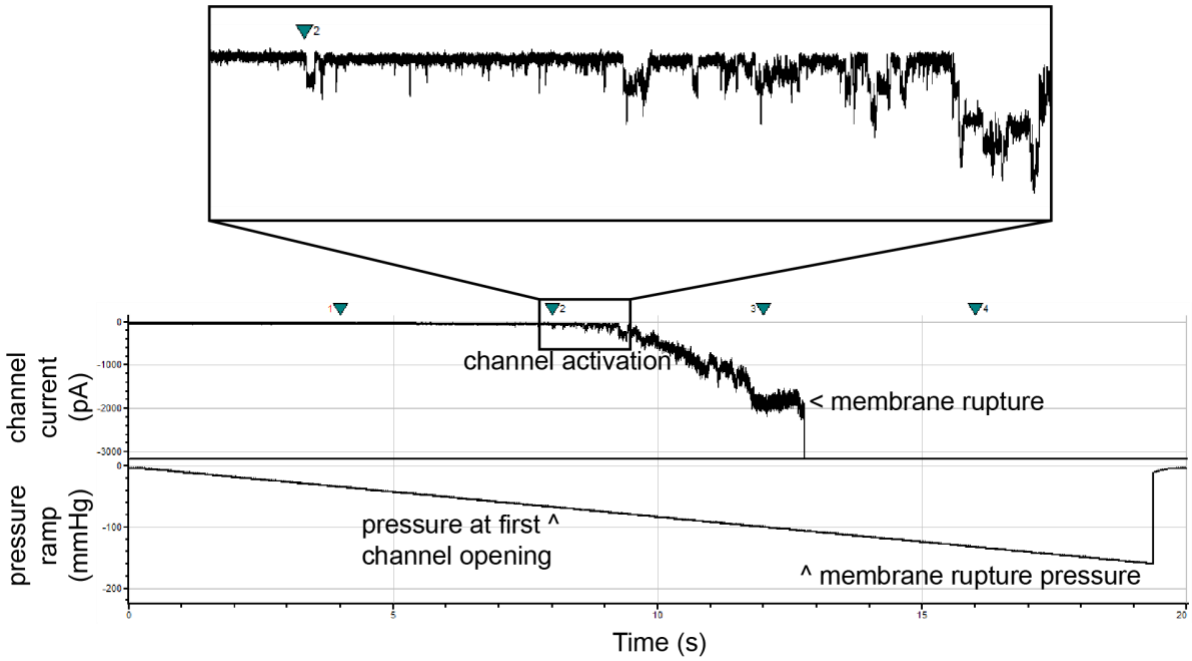

Figure 1–figure supplement 6

Sample data analysis workflow. We calculated MscLG22S pressure sensitivity using an integrated pressure controller to quantify the pressure at which the first MscLG22S channel activated. Higher pressures open more than one channel as demonstrated by multiples of original channel current. Inset demonstrates stochastic channel openings. We applied enough pressure to pop the GPMV membrane to ensure the pressure was high enough to activate mechanosensitive channels in the GPMVs and to enable the quantification of membrane stability.

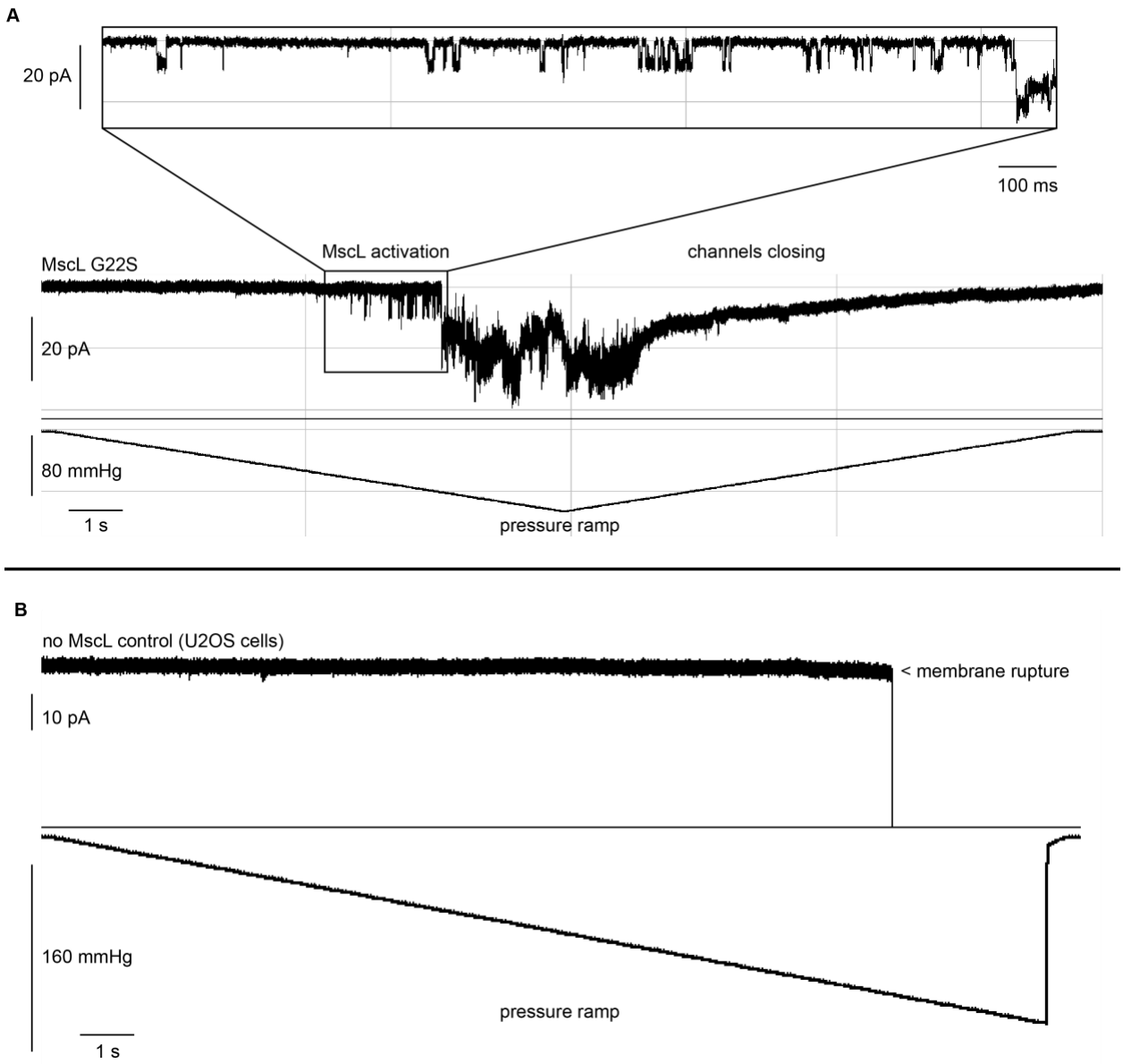

Figure 1–figure supplement 7

Example results of full traces of MscLG22S and no MscL recordings. A) MscLG22S exhibits stochastic activation behavior in response to pressure. When applied pressure is returned to 0 mmHg, MscLG22S closes and current returns to baseline. This suggests that currents observed are due to channel activation and not membrane rupture. B) No MscL control demonstrates no channel currents under MscLG22S activation conditions. Channel currents are not observed up to pressures high enough to rupture the membrane. The open/close pressure ramp in (A) was only used to demonstrate channel closure after pressure reduction, all recordings were performed using this rate of pressure change for all MscLG22s activation calculations.

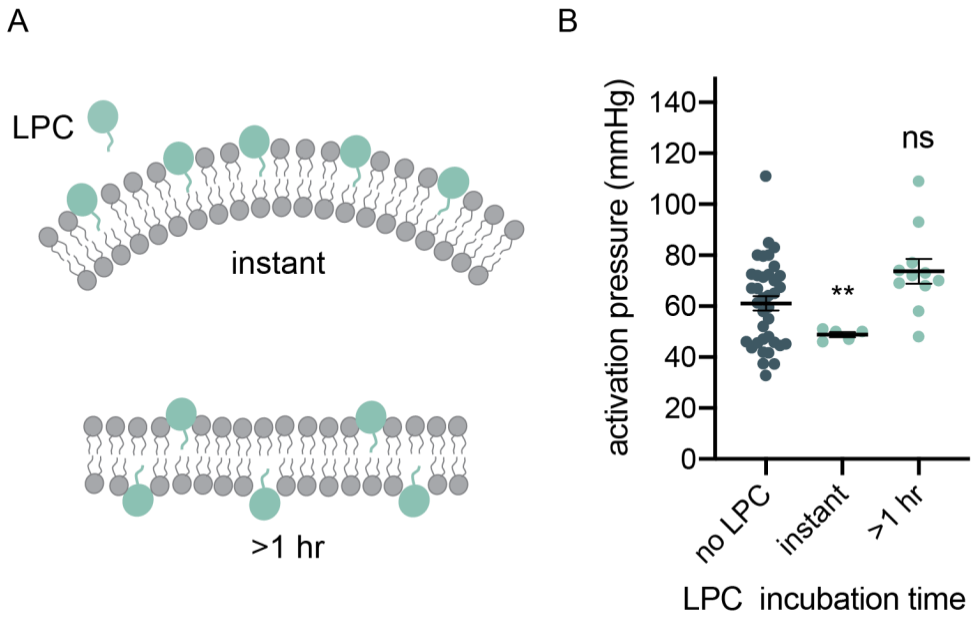

Figure 1–figure supplement 8

Lysophosphatidylcholine (LPC) activation confirms MscLG22S behavior in GPMVs formed from U2OS cells. A) LPC inserts into membranes and induces local changes in curvature on short timescales. These changes in curvature are known to reduce the pressure required to activate MscL (Nomura et al., 2012). On longer timescales, LPC flips and neutralizes curvature where there is no expected effect on MscLG22S activation. B) MscLG22S activation pressure is reduced upon LPC introduction. After incubation for >1hr, LPC does not alter MscLG22S activation pressure as curvature is expected to be neutralized by LPC flip-flop. p-values were generated by ANOVA using Dunnett's multiple comparisons test compared to no poloxamer. ** $p \leq 0.01$, non-significant (ns) $p > 0.05$, $n > 10$.

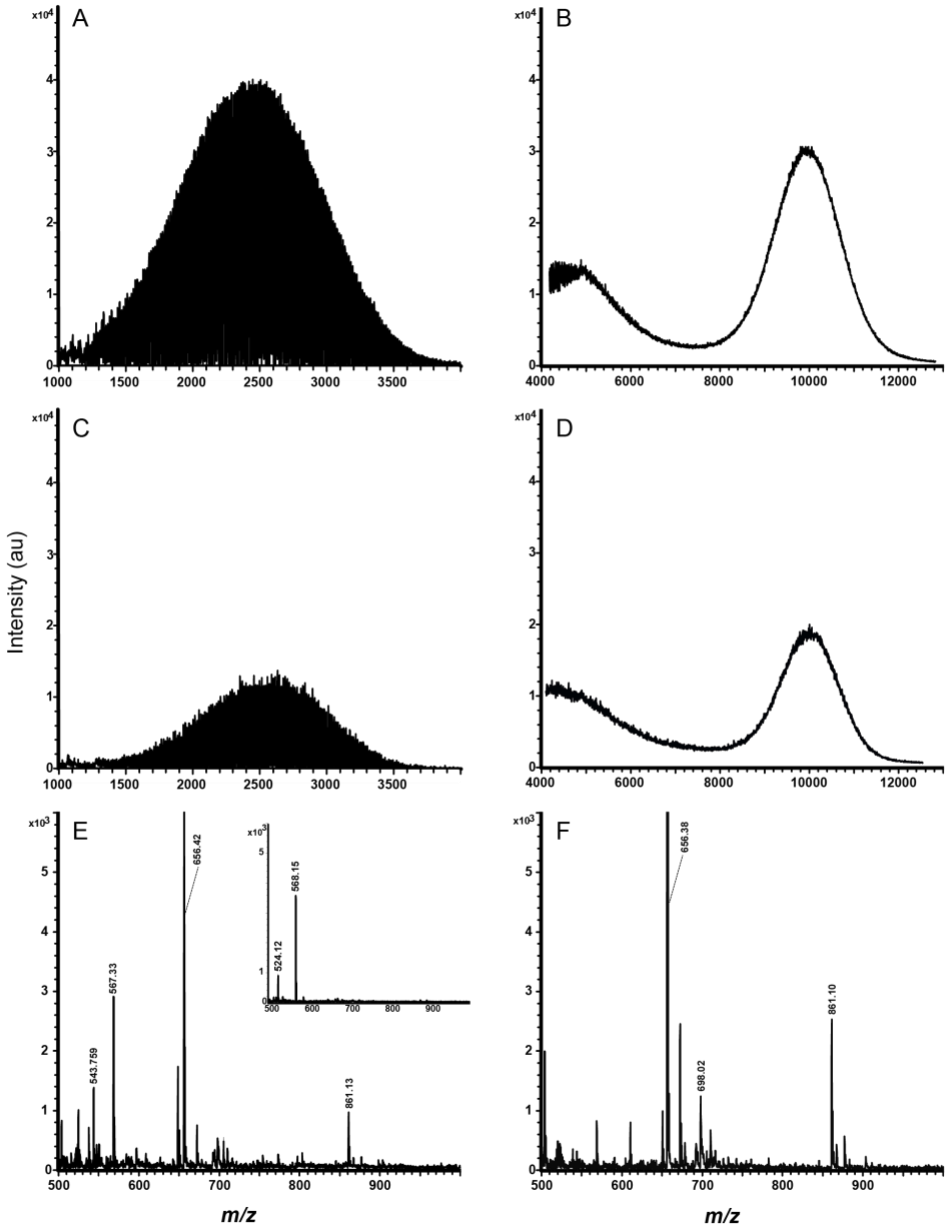

Figure 2–figure supplement 1

MALDI-TOF mass spectra of pure poloxamer A) P124 and B) P188. Samples in panes C–E are poloxamer-integrated P-GPMVs. In separate experiments, data was acquired in the higher mass regions, *m/z* 1000–4000 and *m/z* 4000–12500 to detect C**)** P124 and D**)** P188, respectively. Also, data was acquired in a lower mass region *m/z* 500–1000 to detect E) GPMV lipids of the P124-GPMV and F**)** GPMV lipids of the P188-GPMV. The inset in pane E is the matrix, CHCA, collected in the mass range *m/z* 500–1000.

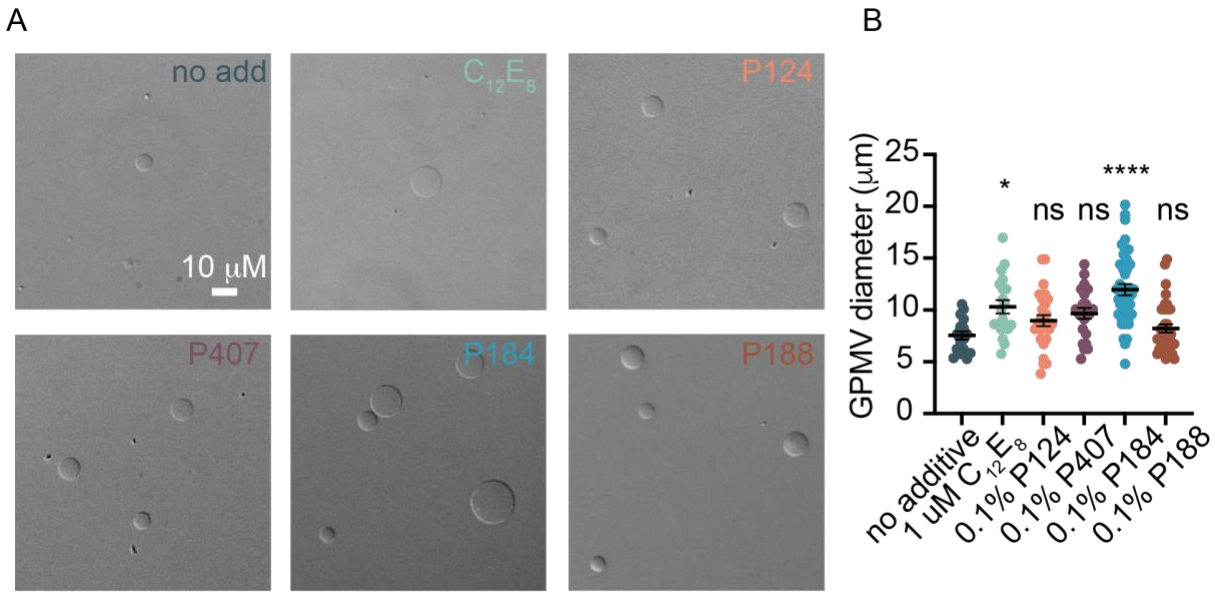

Figure 2–figure supplement 2

GPMV diameter increases in the presence of various poloxamers and a detergent. A) DIC phase contrast micrographs demonstrate the effect poloxamer and detergent ($C_{12}E_8$) on GPMV size. B) GPMV diameter was quantified for all GPMVs large enough to quantify. individual points represent the diameter of a single GPMV, mean and standard error of the mean are plotted. p-values were generated using ANOVA Dunnett's test of multiple comparisons compared to no poloxamer. **** $p \leq 0.0001$, * $p \leq 0.05$, non-significant (ns) $p > 0.05$, $n > 10$.

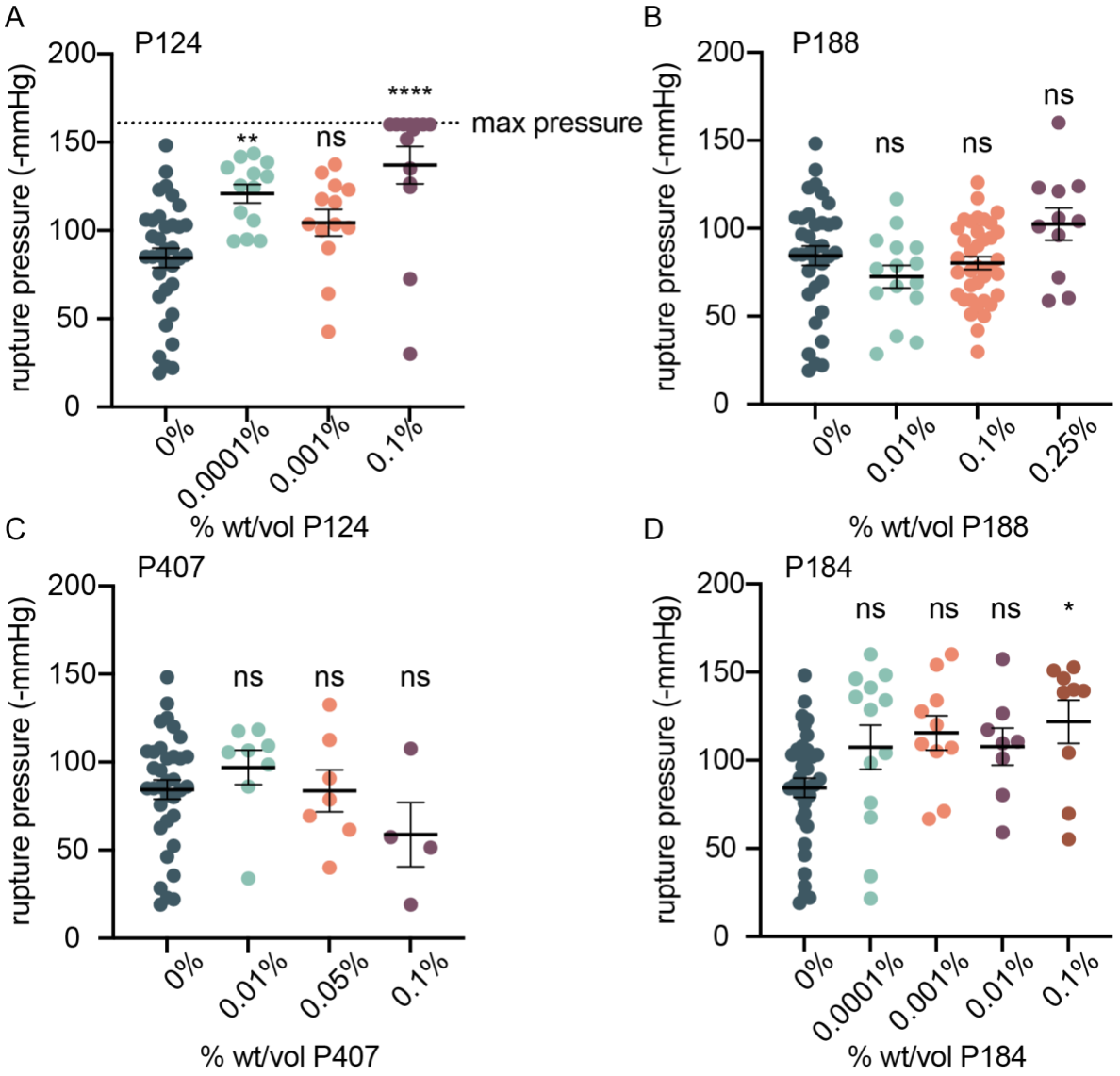

Figure 2–figure supplement 3

Poloxamer effect on membrane stability. We quantified membrane rupture pressure during our electrophysiology recordings of MscLG22S activation to measure if various poloxamers exhibited a strengthening effect on the membrane as has been previously discussed (Zaki and Carbone, 2017). The effect of P124 (A), P188 (B), P407 (C), and P184 (D) were measured, and we observed a membrane strengthening effect in the presence of most poloxamers. However, 407 exhibited a decrease in membrane stability which we hypothesize is due to the large molecular weight of this poloxamer. Each point represents the rupture pressure of a single GPMV, mean is plotted, and error bars represent standard error of the mean. p-values were generated by ANOVA using Dunnett's test for multiple comparisons compared to no poloxamer (0%). * $p \leq 0.05$, non-significant (ns) $p > 0.05$, $n > 10$ for most samples except P407 ($n > 3$) which was prone to popping prior to the initiation of the electrophysiology recording.

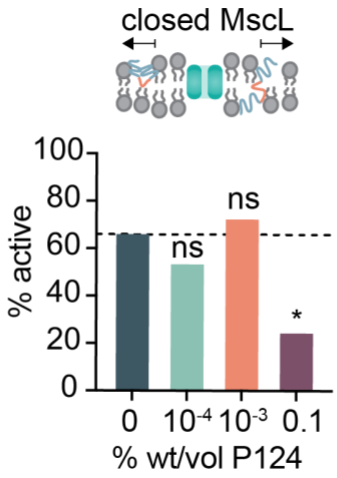

Figure 2–figure supplement 4

P124 prevents MscLG22S activation at high concentrations. Some electrophysiology recordings contained membranes that remained stable in the presence of high pressure (> -80 mmHg), yet MscLG22S did not activate. Recordings in which we observed activation of MscLG22S are presented as % of all recordings for a given condition (% open). The number of recordings in which MscLG22S activation was observed is reported above each bar, n>12. The dashed line represents the percent of recordings in which MscLG22S openings were observed in the absence of poloxamer. p-values were generated using Fisher's exact test comparing the distribution of values to 0% P124, * $p \leq 0.05$, non-significant (ns) $p > 0.05$, n>10.

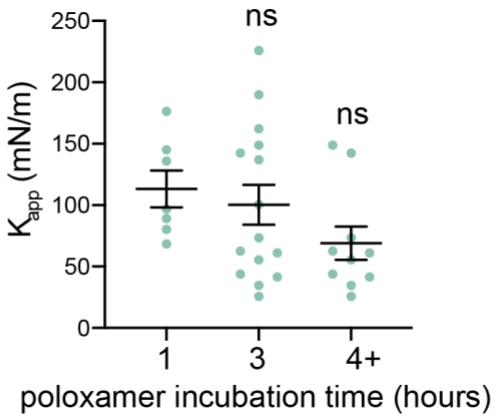

Figure 2–figure supplement 5

Poloxamer incubation time alters poloxamer effect on membrane properties. Incubations longer than 4 hours are required to alter membrane K_A. Samples were incubated with P188 at 4 °C for either 1, 3, or 4 hours and membrane K_A was measured using micropipette aspiration techniques. p-values were generated by ANOVA using Dunnett's test for multiple comparisons compared to 1-hour, non-significant (ns) $p > 0.05$, $n > 6$ independent GPMVs.

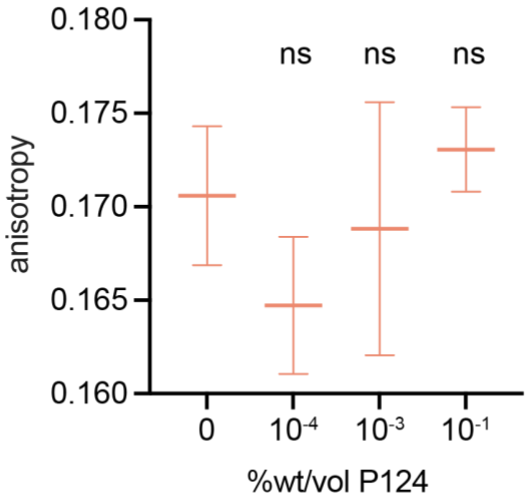

Figure 2–figure supplement 6

P124 Effect on membrane fluidity. Fluorescence anisotropy was used to measure relative differences in membrane fluidity between GPMV membranes containing various amounts of P124. Mean and standard error of the mean are plotted. p-values were generated by ANOVA using Dunnett's multiple comparisons test compared to no poloxamer, non-significant (ns) $p > 0.05$, $n > 10$.

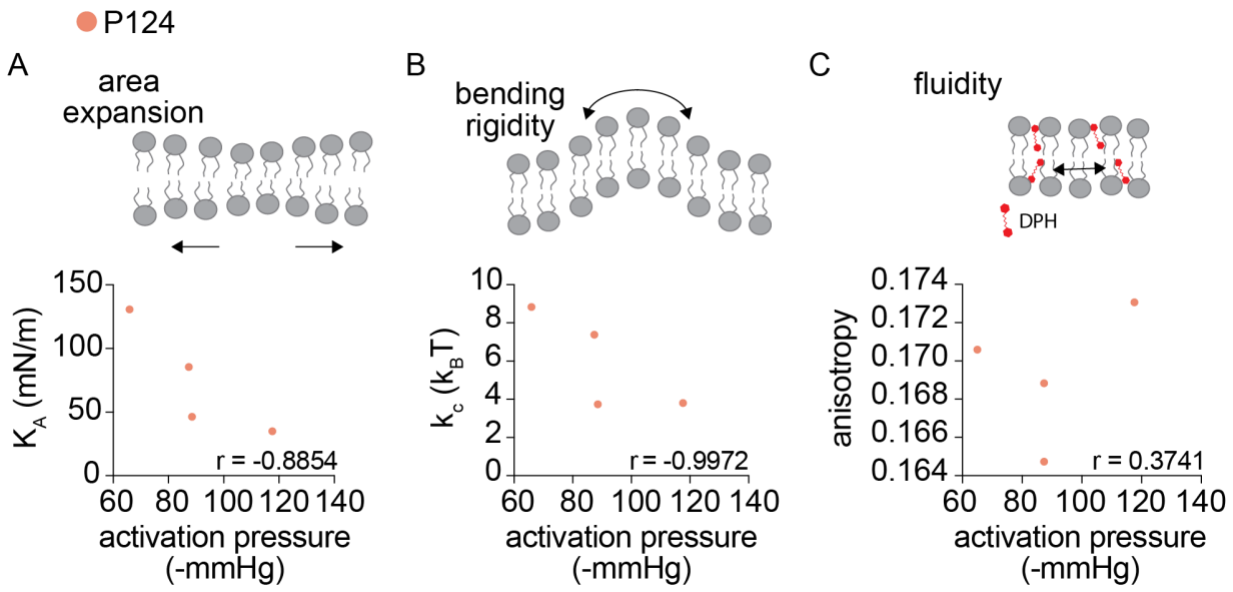

Figure 2–figure supplement 7

Poloxamer P124 alters GPMV mechanical properties. A) P124 decreases K_A and increases MscLG22S activation pressure. K_A is plotted as a function of MscL activation pressure. B) P124 decreases k_c and increases MscLG22S activation pressure. Mean k_c is plotted as a function of mean MscLG22S activation pressure. C) Membrane fluidity does not correlate with MscLG22S activation pressure. Membrane anisotropy was used to measure relative changes in membrane fluidity in the presence of P124. GPMVs were mixed with diphenylhexatriene (DPH) to a final concentration of 50 μM and fluorescence anisotropy was measured using a fluorimeter with fluorescence polarization capabilities. For all plots, Pearson's r was calculated to measure correlation strength, n>10.

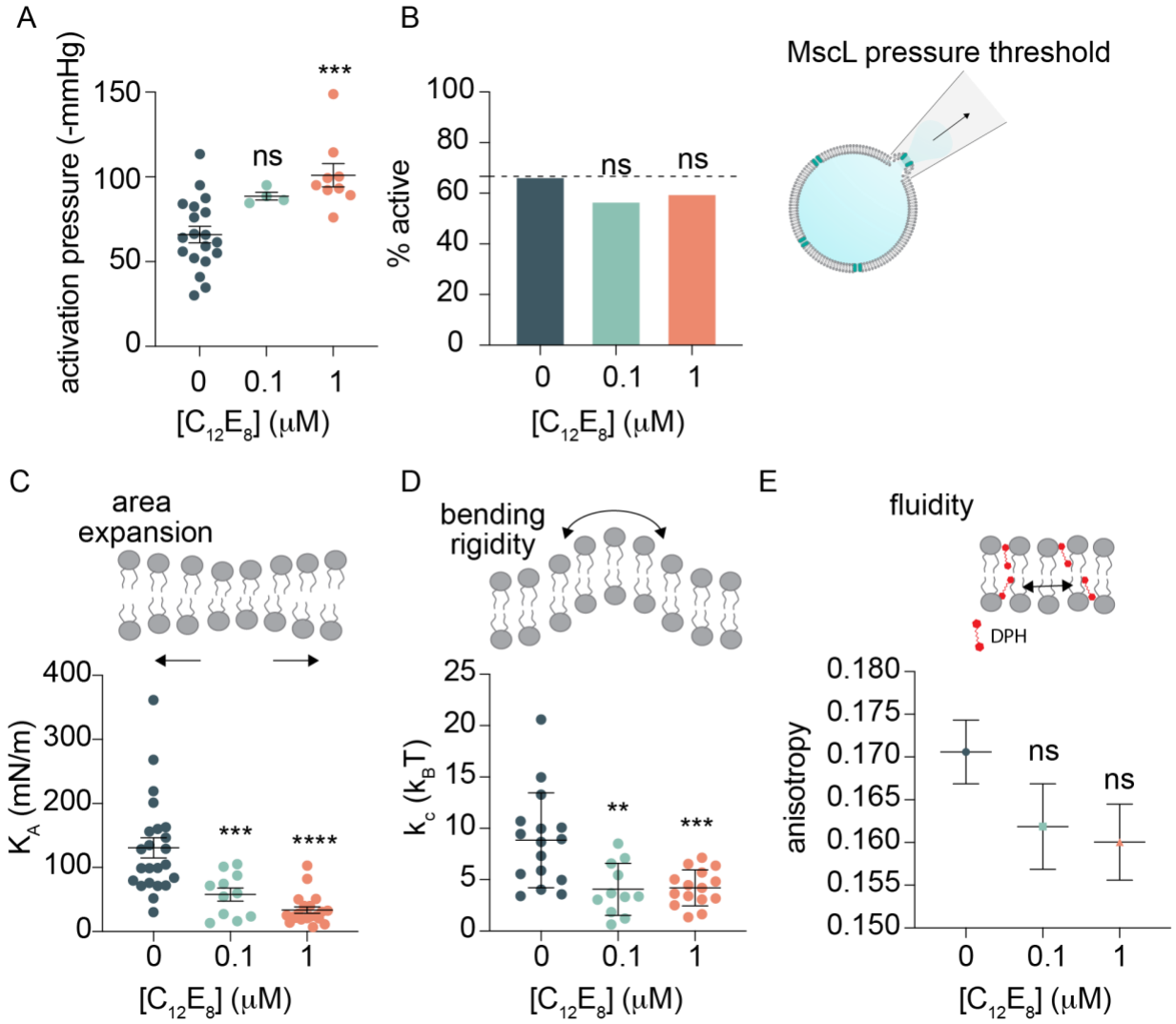

Figure 3–figure supplement 1

$C_{12}E_8$ effect on MscL activation pressure, K_A, k_c, and fluidity. A) $C_{12}E_8$ increases MscLG22S activation pressure with increasing concentration. MscLG22S activation pressure in the presence of $C_{12}E_8$ in the buffer during GPMV formation was measured using patch-clamp electrophysiology and quantified as the pressure at the first channel activation. B) $C_{12}E_8$ did not prevent MscLG22S activation as described in Figure 2 – figure supplement 1. The % of recordings which activated MscLG22S were quantified. p-values were generated using Fisher's exact test compared to 0% $C_{12}E_8$. non-significant (ns) $p > 0.05$, $n > 10$. $C_{12}E_8$ decreased K_a (C), k_c (D) and measured by micropipette aspiration. Points represent individual GPMV measurements which were not repeated. E) $C_{12}E_8$ increased membrane fluidity as measured by fluorescence anisotropy (E). Mean and standard error of the mean for all plots is indicated by the bar and error bars p-values in (A), (C-E) were generated by ANOVA using Dunnett's test of multiple comparisons compared to no $C_{12}E_8$. **** $p \leq 0.0001$, *** $p \leq 0.001$, ** $p \leq 0.01$, non-significant (ns) $p > 0.05$, $n > 10$.

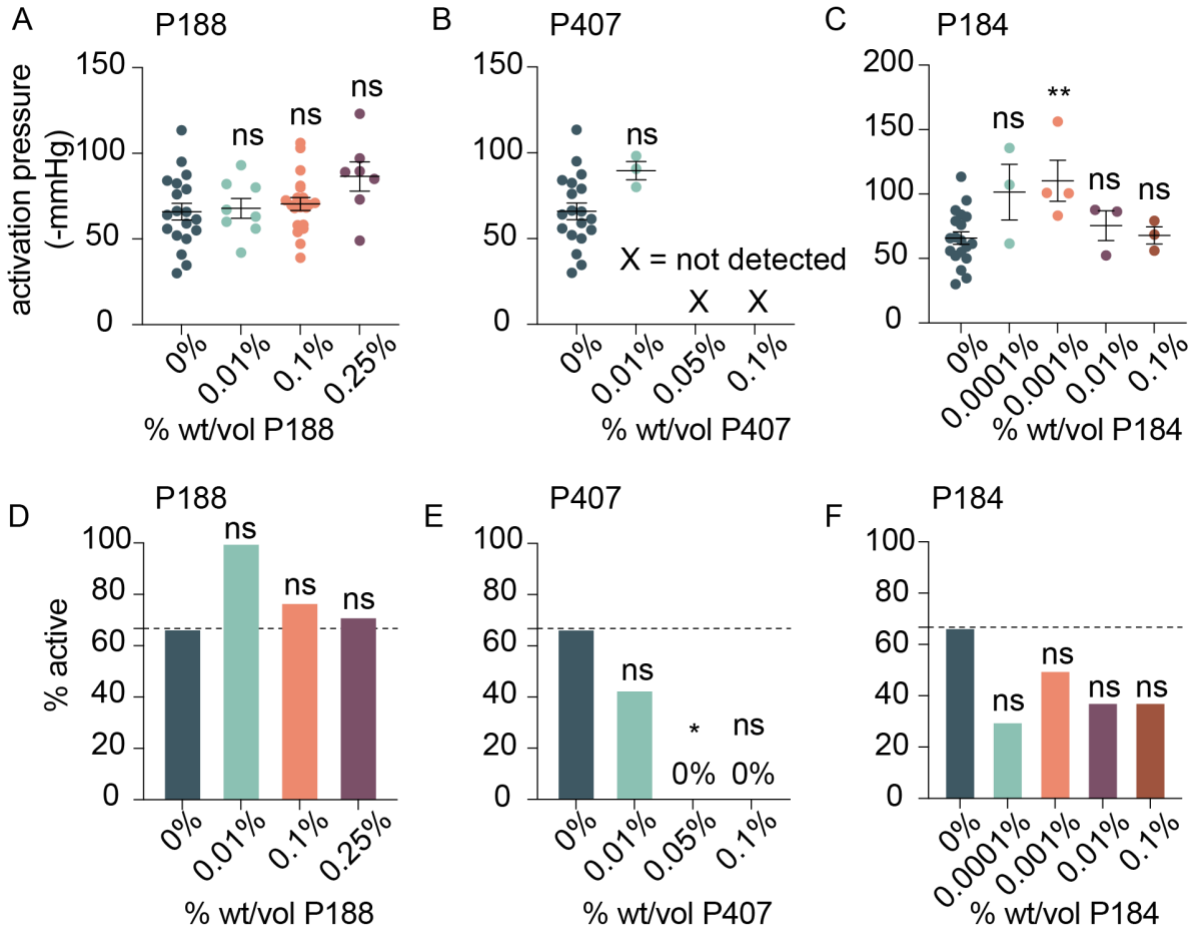

Figure 3–figure supplement 2

MscL activation sensitivity in the presence of various alternate poloxamers. A-C**)** MscLG22S activation pressure is altered by poloxamer identity and concentration. The pressure of MscLG22S first channel opening was calculated in the presence of various poloxamers at increasing concentration of poloxamer in the buffer P124 (A), P407 (B), and P184 (C). Individual points represent independent GPMV recordings. Higher concentrations of P407 (B) destabilized the membrane and led to rupture at pressures lower than the expected activation pressure of MscLG22S. In the small number of P407 GMPVs which were successfully recorded, no active MscLG22S currents were observed Mean and standard error of the mean are indicated by the black bar and error bars. The amount of poloxamer in the GPMV formation buffer is indicated in the plot. p-values were generated using ANOVA Dunnett's test for multiple comparisons compared to no poloxamer (0%). ** $p \leq 0.01$, non-significant (ns) $p > 0.05$, $n > 10$ for all samples except for P407 which led to membrane instability which prevented MscLG22S activation (B). D-E) MscLG22S activation probability is prevented by some poloxamers. P188 (D) had no effect on MscLG22S activation probability while P407 (E) and P184 (F) decreased MscLG22S activation probability. p-values were generated using Fisher's exact test compared to 0% poloxamer. * $p \leq 0.05$, non-significant (ns) $p > 0.05$, $n > 3$.

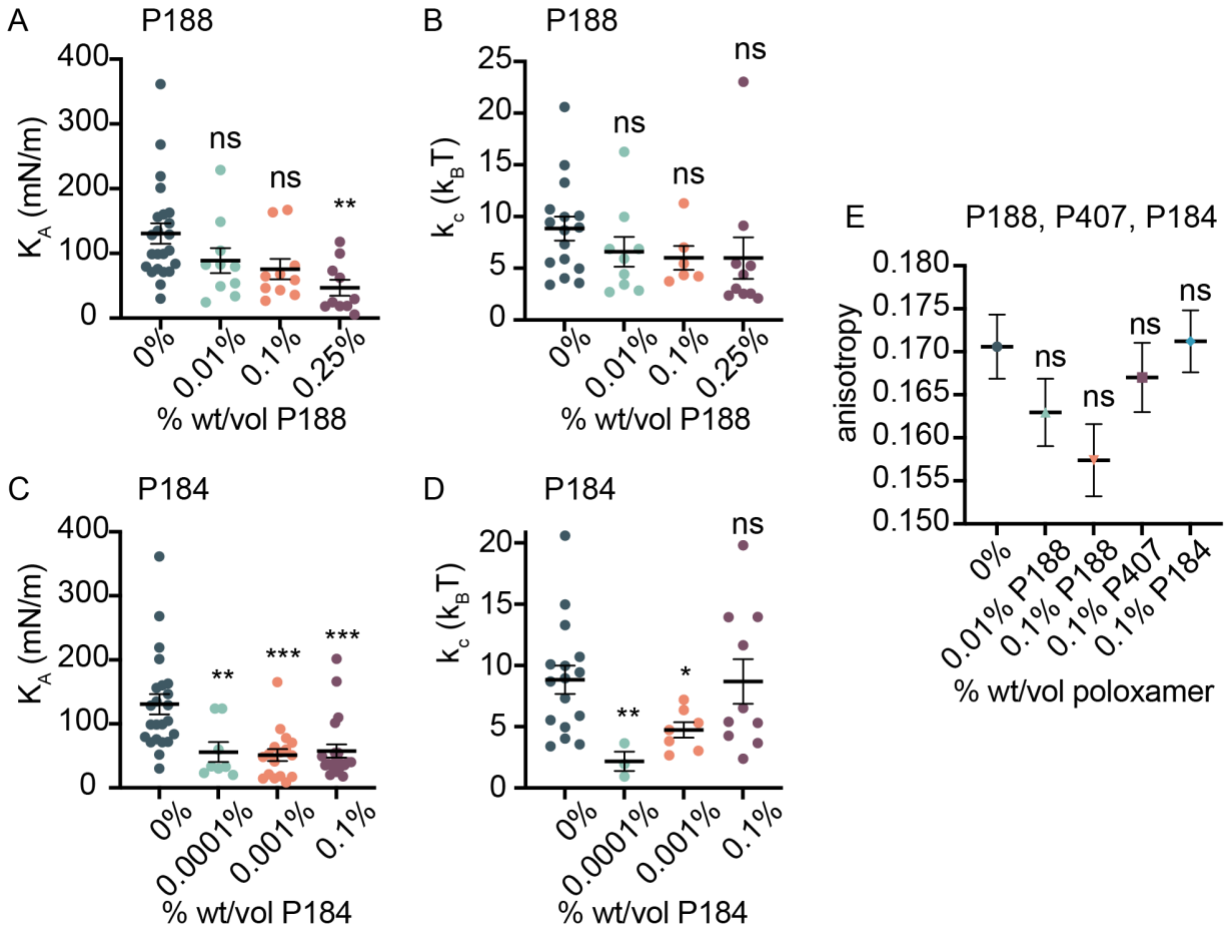

Figure 3–figure supplement 3

Other poloxamer effect on K_A k_c and fluidity. Membrane mechanical properties were measured in the presence of alternate poloxamer molecules, P188 and P184. A, B) K_A and k_c are reduced with increasing P188 concentration. C) P184 generally decreases membrane K_A above 0.0001% wt/vol in the GPMV formation buffer. D) P184 exhibits a non-monotonic effect on membrane k_c where low concentrations decrease k_c, but higher concentrations increase k_c. E) membrane anisotropy was measured in the presence of P188, P407 and P184. no significant differences in membrane fluidity were observed in the presence of these poloxamer molecules.Individual points represent single GPMV measurements, mean and standard error of the mean are plotted as a black bar with error bars, pH 7.4. p-values were generated using ANOVA Dunnett's test for multiple comparisons compared to no poloxamer (0%). *** $p \leq 0.001$, ** $p \leq 0.01$, * $p \leq 0.05$, non-significant (ns) $p > 0.05$, $n > 10$.

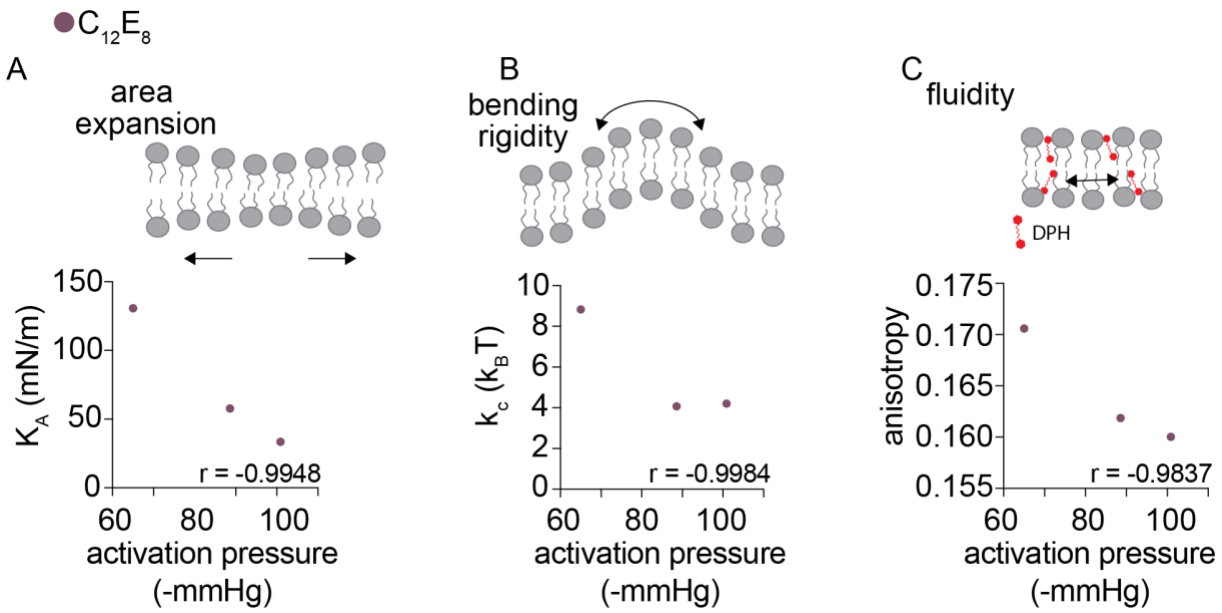

Figure 3–figure supplement 4

A non-ionic detergent decreases MscL sensitivity and alters membrane properties similar to poloxamer. A) $C_{12}E_8$ increases the pressure required to activate MscLG22S. $C_{12}E_8$ was introduced to GPMVs during formation in buffer at the indicated concentration. Mean activation pressure and standard error of the mean is plotted. p-values were generated by ANOVA using Dunnett's multiple comparisons test compared to no poloxamer. non-significant (ns) $p > 0.5$, *** $p \leq 0.001$, $n > 10$. B) $C_{12}E_8$ decreases area expansion modulus and increases MscLG22S activation pressure. K_a was measured using micropipette aspiration. Mean K_a is plotted as a function of mean MscLG22S activation pressure are plotted for each concentration of $C_{12}E_8$. C) $C_{12}E_8$ decreases membrane k_c and increases MscLG22S activation pressure. Mean k_c is plotted as a function of mean MscLG22S activation pressure. B) Membrane fluidity and MscLG22S activation pressure are increased in the presence of $C_{12}E_8$. Mean fluorescence anisotropy of DPH is plotted as a function of MscLG22S activation pressure. Decreased anisotropy indicates a relative increase in membrane fluidity. For all plots, Pearson's r was calculated to measure correlation strength, n>10.

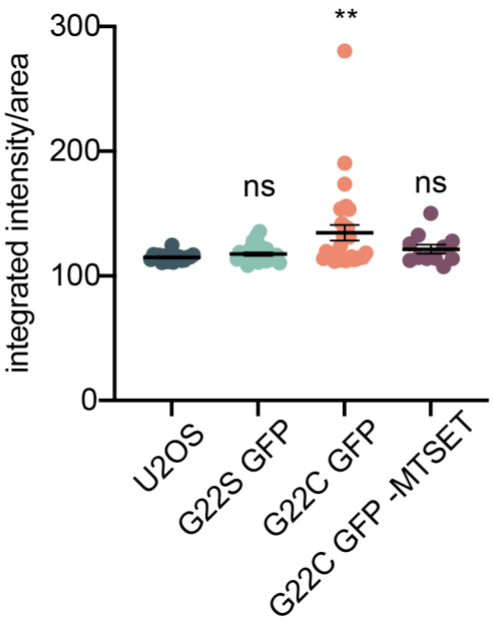

Figure 4–figure supplement 1

Validation of GPMV calcium influx assay. MscLG22C is a chemically-activatable mutant of MscL which opens in the presence of MTSET through binding to cysteine groups which induces forced hydration of the hydrophobic gate. Calcium and MTSET were added to GPMVs formed from cells incubated with Fluo4 Ca^{2+} indicator and Ca^{2+} influx was detected as an increase in Ca^{2+} fluorescence and was quantified as integrated intensity/area. GPMVs formed from untransfected cells (U2OS) and MscLG22S treated with MTSET, and MscLG22C GPMVs not treated with MTSET (G22CGFP(-MTSET)) did not exhibit increases in fluorescence in response to Ca^{2+}. p-values were generated by ANOVA compared to no MscL (U2OS). ** $p \leq 0.01$, non-significant (ns), $p > 0.05$, $n > 10$ independent GPMVs.

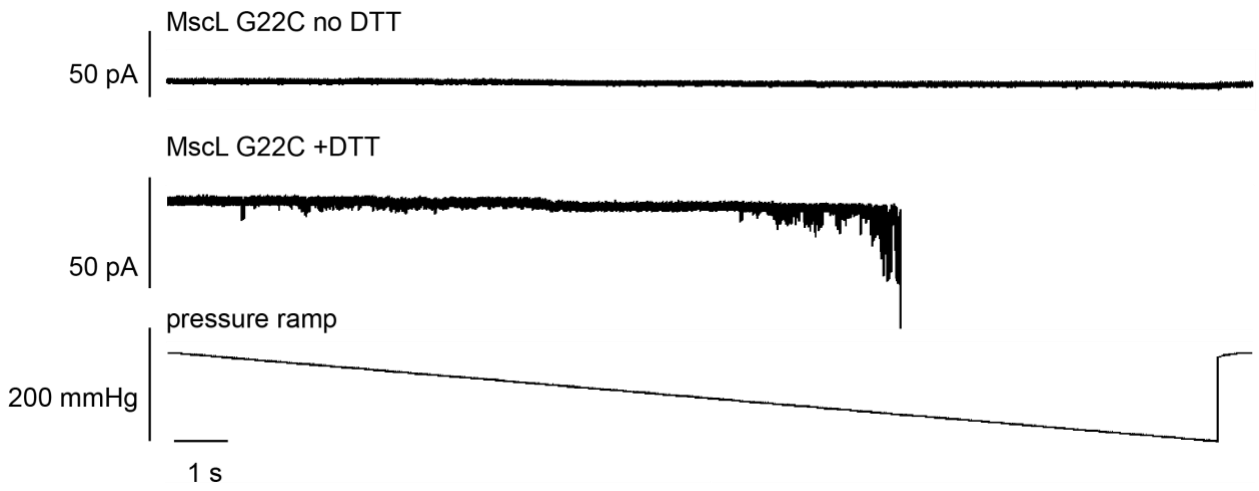

Figure 4–figure supplement 2

MscLG22C pressure sensitivity is restored in the presence of DTT. The chemically activatable mutant, MscLG22C, used in Ca^{2+} imaging assays was further characterized using patch-clamp electrophysiology to confirm channel activity. Without DTT (top) the channel is not mechanically activatable as described previously (Levin and Blount, 2004) due to disulfide bonds which prevent channel opening. In the presence of DTT, channel mechanosensitivity is restored and stochastic channel activation is observed with increasing pressure.

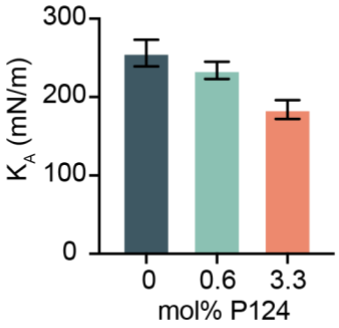

Figure 4–figure supplement 3

Coarse-grain molecular dynamics simulations confirm the effect of P124 on membrane elasticity. Membrane KA was measured at increasing concentrations of P124 and was found to decrease similar to experimental results. Error bars represent standard error of the mean, n=3.

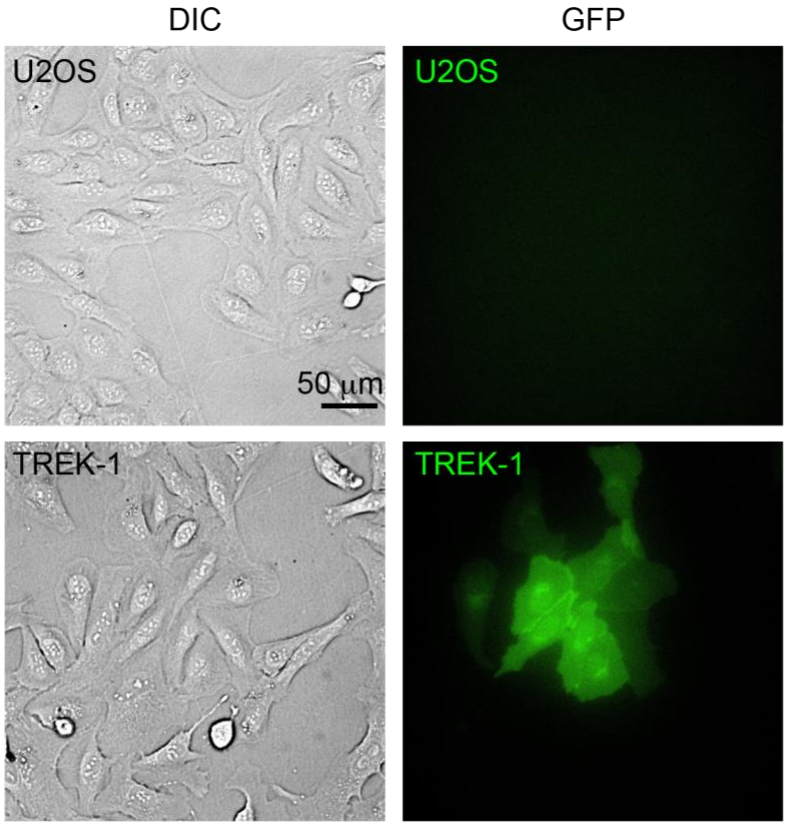

Figure 5–figure supplement 1

U2OS cells stably expressing mTREK-1. mTREK-1 tagged with GFP localizes to the membrane as shown in GFP images. DIC images are shown to demonstrate cell boundary and confluency.

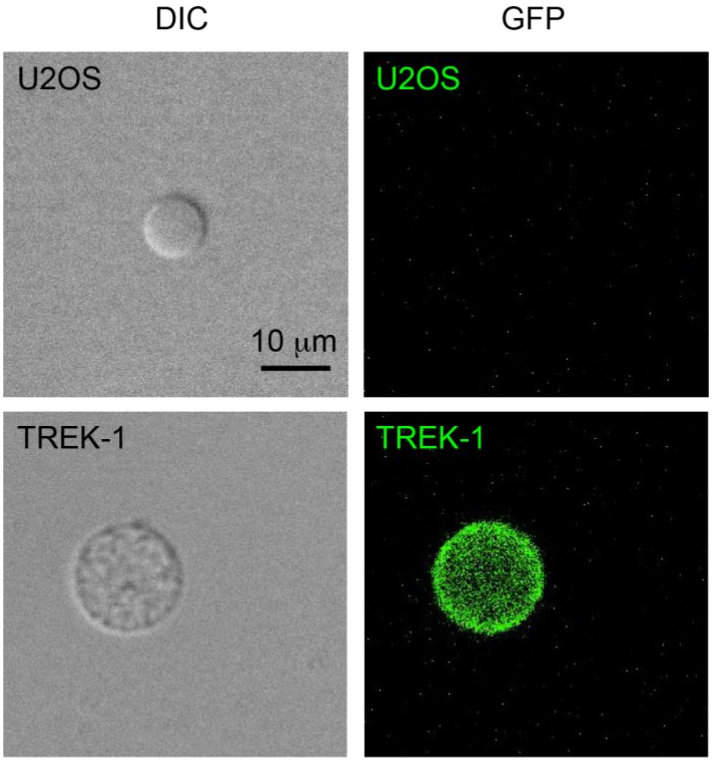

Figure 5–figure supplement 2

TREK-1 is retained in GPMV membranes. TREK-1 tagged with GFP is localized to the GPMV membrane. no GFP signal is detected in untransfected cells (U2OS).

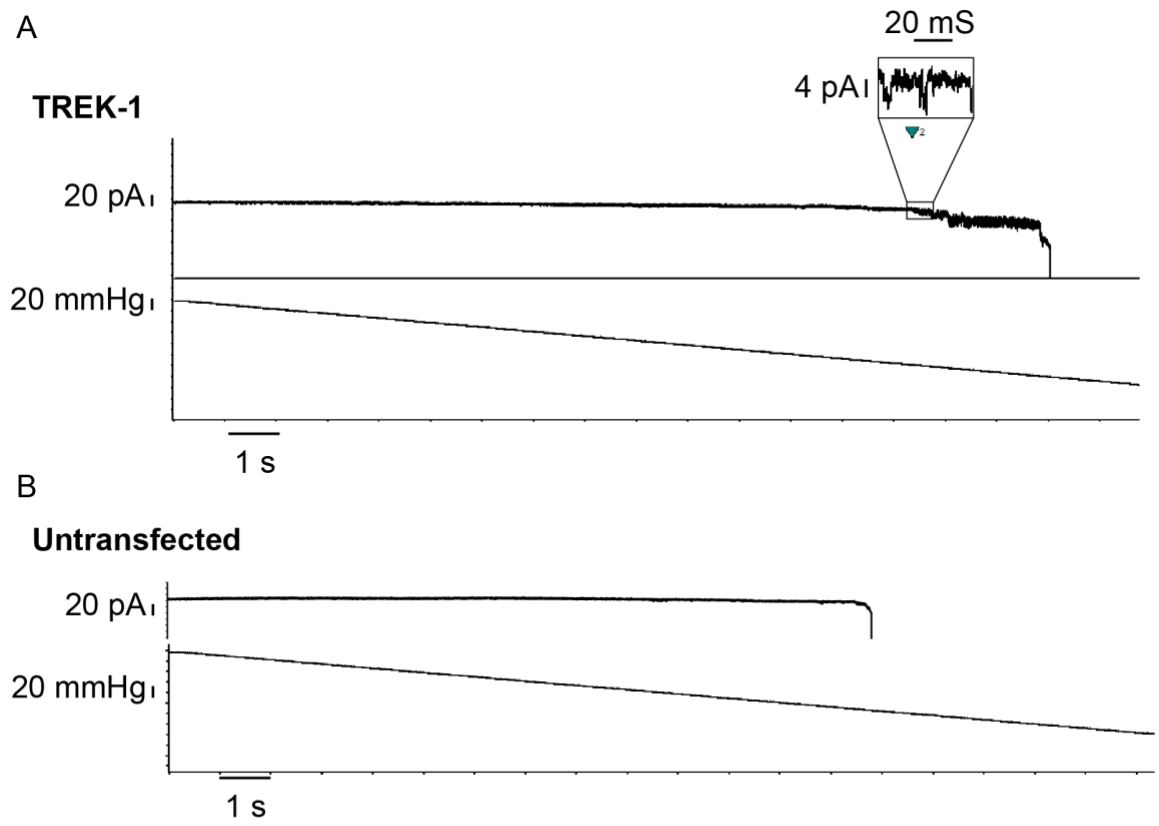

Figure 5–figure supplement 3

TREK-1 mechanosensitive currents are only observed in GPMVs formed from stable cells expressing TREK-1. A) We observed TREK-1 activation where single channel currents were ~4.5 pA at -50 mV. TREK-1 activation was observed in most patches above -30 mmHg. B) To further confirm that we observed TREK-1 channels in our electrophysiology recordings, we performed patch-clamp electrophysiology on GPMVs formed from U2OS cells that were untransfected, referred to as untransfected GPMVs, under identical conditions as our TREK-1 recordings which required higher holding potentials to observe single channels due to the smaller conductance of TREK-1 compared to MscLG22S. We applied enough pressure to pop the GPMV membrane to ensure the pressure was high enough to activate any native mechanosensitive channels in the GPMVs. We did not observe any channels in untransfected GPMVs before membrane popping. Recordings are performed at -50 mV in asymmetric potassium buffer conditions. Bath solution was composed of 10 mM HEPES, 150 mM KCl, 2 mM $MgCl_2$ for excised-patch recordings on TREK-1 with outward rectifying potassium currents. n > 6 recordings on independent patches.